GEOLOGICAL SURVEY OF CANADA COMMISSION GÉOLOGIQUE DU CANADA

Contract Report

D.S.S. #23445-0-0164/01-XSA

Analysis and Interpretation of Seismic Data from the Western Canada Continental Margin.

Part 2: Multichannel Reflection Data across the Vancouver Island Margin.

Marine Multichannel Seismic Reflection Survey across the Northern Cascadia Accretionary Prism

G.D. Spence, R.D. Hyndman, S.G. Langton,
E.E. Davis, and C.J. Yorath

Contractor : Department of Physics and Astronomy
University of Victoria
Victoria, B.C. V8W 3P6

Investigator : G.D. Spence
Research Assistant : S.G. Langton

April 1991

Canada

Open File 2391

accompanying report

INTRODUCTION

From September 1 to 15, 1989, a marine multichannel seismic survey was shot off the west coast of Vancouver Island. A total of 13 lines (722 Km) of reflection data was obtained over the Tofino Basin beneath the continental shelf, and over the deformation front of the accretionary wedge (see Fig. 1). The data were collected by Digicon (Canada) Inc., using the vessel M/V Geo Tide equipped with Digicon's DSS-240 cable system. The data were processed in Calgary by Geophoto Inc. Both data and processing were under contract to the Geological Survey of Canada as part of site surveys for the scientific international Ocean Drilling Program.

The objective of the program was to determine the structural architecture and tectonic history of the Vancouver Island continental margin. Of particular interest were (1) the regional structure and stratigraphy of the Tofino Basin and of the deeper structures within the accretionary prism which provide basin controls; (2) the three dimensional variation in fold and thrust structures at the deformation front; (3) physical properties related to the shallow bottom-simulating reflector beneath the lower slope, previously interpreted as the base of a methane hydrate layer; (4) the nature of the basal thrust or detachment that could produce large earthquakes.

DATA RECORDING

The 144 channel system recorded data for 14 sec. at a sampling rate of 4 msec. The 3600 m. cable, towed at a depth of 12 m. (±2 m.), was configured at a group interval of 25 m., with 14 hydrophones in each group. The seismic source was a tuned airgun array fired at 50 m. intervals to provide 36 fold data. The array was made up of 4 strings of 10 guns each (3 active strings and one spare), with a total airgun volume of 7820 cu. in. operating at 1900 p.s.i. and at a depth of 10 m. (±2 m.). The offset from the centre of the gun array to the centre of the first group was 183 m. Navigation for the survey was by Starfix augmented by satellite navigation.

A total of 5 sonobuoys were deployed to record airgun arrivals at offsets of up to 20 km or more. The sonobuoy signal was recorded on one channel of an analog tape recorder, and the time break signal from the airgun trigger system was recorded on another channel. The 5 sonobuoy locations were in the region of the deformation front on lines 7, 10 and 11, on the upper slope at the start of line 7, and in the Tofino Basin on line 2.

Four of the lines which crossed the continental shelf (lines 1, 2, 6 and 9) were also recorded by the University of British Columbia at two or more land refraction sites near the end of each

line. Absolute times were required to determine both the shot instant and the refraction arrival times. Shot times were obtained by using the airgun time break signal to trigger a GOES satellite clock, which then output the shot time to a dedicated hard disk.

SEISMIC DATA PROCESSING

A. Normal Sequence

After tests on data the following processing scheme was adopted:

1. First break mute

2. True amplitude recovery - The data were corrected for spherical divergence by multiplication by a factor proportional to time. In addition, an exponential gain factor was applied to compensate for inelastic attenuation, using a factor of 3.5 db/s for a time of 0-6 s below the water bottom.

3. Velocity filtering of coherent linear noise - in the common shot domain with a band pass of:
   -7 msec./trace to 15 ms/trace at water depths of less than 1000 m.
   -7 msec./trace to 14 ms/trace at water depths of greater than 1000 m.

4. Designature. - A theoretical source signature, based on the geometry and depths of the source and receiver arrays, was removed from the data. A zero-phase signal was output. One filter was applied to all 144 traces on a shot gather. Velocity filtering was applied prior to designature to improve signal coherency, so that less distortion would be produced by the designature procedure.

5. Velocity analysis (VELSCAN) - Locations for demultiple velocity functions were handpicked by the Geophoto processors.

6. FK demultiple. - The procedure was applied to the data in both shallow and deep water to remove the water bottom multiples and their pegleg multiples. Laterally varying velocity functions were used.

7. Velocity analysis - Locations for the analysis were handpicked by the G.S.C., at a nominal spacing of 3 Km. Seven velocity functions were input and analyses were run for sub-surface times leass than 10.0 s. Output included NMO corrected panels plus velocity function stacks. Velocity scans were applied to nine consecutive depth points using a time window of 100 ms, and within each window values were recorded for velocity, dip, dip-corrected velocity, and amplitude relative to a calibration pulse located at the picked water bottom time.

8. Deconvolution - offset and time variant from water bottom.

9. Equalization - 9000 ms design gates.

10. Statics - Correction for shot and receiver depth.

11. Normal moveout corrections.

(a) Deep Ocean Basin

Velocity analysis results were applied down to the strong basement reflector at approximately 2 s below the seafloor. Below the basement time B, the following ocean crust velocity function (based on Waldron & Clowes, 1989; H. White & R. Clowes, pers. comm., 1990) was used:

(i)	B to B+0.67 s	linear increase to 6.85 km/s	~2 km thick
(ii)	B+0.67 s to B+1.9 s	6.85 km/s	~4 km
(iii)	B+1.9 s to bottom	8.0 km/s	

(b) Continental Shelf

Velocity analysis results were used to 3.5 s. For greater depths, a generalized deep velocity function for the continental shelf (based on studies by Waldron & Clowes, 1989; Spence et al. 1985; Taber & Smith, 1985) was applied:

(i)	3.5 to 4.7 s	4.95 km/s	3 km thick
(ii)	4.7 to 5.85 s	5.25 km/s	3 km
(iii)	5.85 to 6.9 s (i.e. B) or to B if shallower than 6.9 s	5.55 km/s	3 km
(iv)	B to B+0.75 s	6.00 km/s	2 km
(v)	B+0.75 to B+1.9 s	6.85 km/s	4 km
(vi)	B+1.9 to bottom	8.00 km/s	

(c) Continental Slope

Deep velocities were interpolated between the deep ocean and continental shelf velocity functions.

12. Common depth point stacking - 36 fold diversity power stack.

13. Deconvolution - To further attenuate multiples, predictive deconvolution after stack was applied, with a filter length of .3 × two way time water depth and a gap length of .9 x two way water time. Autocorrelation start/end times were -50/9000 ms.

14. FK migration (dip limit 45 degrees). Input velocities were hand smoothed NMO functions, reduced by 10% to prevent overmigration.

15. Time variant filter :

water bottom datum	8,12 / 36,44 Hz
+2.0 s	3, 6 / 26,34 Hz

16. Time variant scaling (water bottom datum; start time -25 ms)
square root balance : gates 200, 200, 500, 1000, 5000 ms
trace equalization : gates 2000, 4000, 6000 ms

B. Processing Sequence for AVO Analysis

On lines 4, 8, 10 and 17, sections 4 to 5 km in length were chosen for a study of amplitude variation with offset (AVO). Processing for the AVO study was carried out by Geophoto (Halliburton Geophysical Services, Inc.). The main steps of the pre-AVO processing sequence are outlined below:

1. Reformat to internal HGS format (0-6.0 s only)
2. Geometry file creation
3. Pre-deconvolution mute
4. Bad trace mute
5. Designature
6. Spherical divergence correction
   - amplitude proportional to time
   - no exponential attenuation applied
7. Sort to common depth points
8. Prestack migration (45° finite difference algorithm)
   - near 24 traces only (2/3 of the spread)
9. Velocity analysis
   - one analysis per kilometre, 11 CDP's per analysis
   - eight velocity functions
10. P-wave stacks
   (a) full stack (0-1950 ms at BSR)
   (b) near 1/3 substack (0-750 m at BSR)
   (c) middle 1/3 substack (750-1350 m at BSR)
   (d) far 1/3 substack (1350-1750 m at BSR)

The AVO process is based on the simplified Zoeppritz equations dereived by Shuey (1985). The following products were output:

(a) zero-offset section
(b) AVO raw slope section
(c) AVO absolute value slope section
(d) Poisson's ratio indicator section
(e) error estimate sections

In the AVO analysis, a linear fit is determined at each time sample of amplitude versus the angle of incidence. The "zero-offset stack" represents the intercept amplitude for the linear fit and the "raw slope section" represents the gradient. The "absolute value section" indicates whether the absolute values of the amplitude are increasing or decreasing with offset, i.e. without regard to the sign of the amplitude. The final output of the AVO process are apparent Poisson's ratio contrasts between layers, based on the assumption that the average Poisson's ratio of the layer above the interface and the layer below is 0.25.

C. Processing of the Sonobuoy Data

Using the recorded airgun time break as a trigger, the analog data were digitized at a sample rate of 4 ms and a nominal record length of 16 s. The data were written to tape in SEGY format, using the Lithoprobe Data Storage convention to record refraction parameters (Spencer et al., 1989). Because the sonobuoy drifted in the currents, shot-receiver distances had to be calculated from the times of the water-wave arrivals. The Institute of Ocean Sciences provided velocity-depth profiles in the water column, collected on cruises near the time and location of the reflection survey (J. Linguanti, pers. comm., 1990). The sonobuoy data were bandpass filtered from 5-75 Hz and record sections prepared. Data tapes and record sections are available.

SEISMIC DISPLAYS

Final stacks were produced at a scale of 3.0 cm/s vertically with every second CDP trace plotted at 20 traces/cm. With a CDP interval of 12.5 m, this results in a horizontal scale of 1:50000.

Three migrated time sections were produced:

(1) 2.0 cm/s vertically and every second trace plotted at 20 traces/cm (1:50000 horizontal scale).
(2) 6.0 cm/s vertically and every second trace plotted at 20 traces/cm (1:50000 horizontal scale).
(3) 6.0 cm/s vertically and every trace plotted at 20 traces/cm (1:25000 horizontal scale).

Migrated depth sections were also produced with every second trace plotted at 20 traces/cm (1:50000) and vertical scales of

(1) 2.0 cm/km, for a vertical exaggeration of 1:1
(2) 4.0 cm/km, for a vertical exaggeration of 2:1

The seismic displays included in this report are the final stacks and the migrated time sections, plotted at 3.0 cm/s vertically and every second trace at 20 tr/cm. The horizontal scale is 1:50,000, and the vertical exaggeration is 1:1 at a velocity of 3.0 km/s (i.e. varying from approximately 2:1 at the seafloor to 1:2 for a velocity of 6.0 km/s which is reached within the ocean crust, beneath the inner continental shelf, or deep beneath the outer continental shelf).

See Appendix 1 for a listing of the seismic plots presented in this report, including the line numbers and shot point ranges for each of the seismic displays.

SHOT POINT LOCATION DATA

The shotpoint location map is at a scale of 1:250000. A listing of the coordinates of every 50th shotpoint, plus the start and end times of recording for each line is given in Appendix 2.

DATA TAPES

All data tapes are stored by the Geological Survey of Canada at the offices of the Federal Public Archives in Vancouver. Tapes include the original field data, demultiplexed SEGY data, and the common depth point gathers prior to NMO removal. A listing of all tapes is given in Appendix 3.

REGIONAL GEOLOGICAL AND TECTONIC SETTING

At the western Canadian convergent margin, the Juan de Fuca and Explorer plates subduct beneath the North American plate at rates of about 47 and 20 km/Ma, respectively (Riddihough, 1977, 1984; Riddihough and Hyndman, 1991). Above the downgoing oceanic plate, the Cascadia accretionary wedge has formed by deformation, offscraping and underplating of rocks beneath the overriding continental plate. Beneath the continental shelf off Vancouver Island lies the Tofino Basin, with a maximum width of about 60 km and a length of 200 km. The Tofino Basin comprises Paleogene and Neogene clastic rocks (Shouldice, 1971) that have been penetrated by six exploratory wells (Fig. 1).

High quality multichannel data were collected across Vancouver Island by the Lithoprobe programme in 1984 (Clowes et al. 1987, Green et al. 1986,1987), and across the continental shelf and slope by the Geological Survey of Canada in 1985 as part of its Frontier Geoscience programme (Yorath et al., 1987; Davis & Hyndman, 1989; Hyndman et al., 1990; Davis et al., 1990; Hyndman and Davis, 1991). Integrated with previous geological and geophysical results, the seismic data have delineated the extension of two narrow terranes from Vancouver Island to beneath the continental shelf. The Pacific Rim Terrane on southern and western Vancouver Island consists of Triassic volcanic rocks and Jura-Cretaceous melange. The Crescent Terrane, exposed on southern Vancouver Island and the Olympic Peninsula, comprises Eocene oceanic basalts. The basalts have been penetrated by the Tofino Basin exploratory wells, and can be traced by a magnetic high , parallel to the margin for over 150 km (see Fig. 1 and Hyndman et al., 1990).

The sediment section entering the subduction zone comprises a fine grained hemipelagic unit underlying a thicker, more reflective Pleistocene turbidite section. Near the deformation front, deformation is accomplished by folding and faulting, with thrust

faults and related anticlines occurring at a spacing of about 5 km (Davis & Hyndman, 1989). In some cases the thrust faults appear to penetrate almost completely through the sediment section to near the igneous ocean crust, implying that few sediments are available for underplating or deep subduction. Beneath the lower continental shelf, a shallow "bottom simulating reflector" is observed throughout the region. This reflector has been interpreted as the base of a methane hydrate layer, which can be used as a measure of temperature and heat flow, and possibly as a semi-quantitative indicator of fluid flow from within the accretionary prism (Davis et al., 1990; Hyndman & Davis, 1991).

PRELIMINARY RESULTS

A. General Structure

A preliminary description of some of the prominent features of the new seismic lines are presented in Spence et al. (1991), a copy of which is attached to this report.

B. Bottom Simulating Reflector: Velocities and AVO Analysis

Figure 2 shows results of velocity analyses run every kilometre on the four AVO line segments. Superimposed on the observed velocities are RMS velocity-depth curves for a series of models contianing a high-velocity hydrate layer of variable thickness. The velocity in the hydrate increases uniformly from the background sediment value to 2.1 km/s. The modelled velocities are generally consistent with the observed data, but the scatter in the data is too large to distinguish between layer thicknesses of 200 m or less. Models were also run for which the maximum velocity in the hydrate was 2.5 km/s, and results indicate that the thickness of the hydrate velocity gradient layer is at most 60-120 m.

On common depth point gathers, the variation of amplitude with offset at the BSR was measured at several locations in the AVO dataset. Averages for the observed amplitudes are shown in Figures 3 and 4. The CDP gathers have been corrected for geometrical spreading, and the measured amplitudes were subsequently corrected for directivity of the receiver and source arrays.

Theoretical amplitudes are also shown in Figures 3 and 4 for a variety of velocity models. Model amplitudes were calculated using the reflectivity method (Fuchs & Muller, 1971), which is not restricted to angles less than the critical angle as is the Zoeppritz approximation of Shuey (1985). Consistent with the observed amplitudes, reflectivity values were multiplied by a factor proportional to time so that geometrical spreading is backed out. Two sets of models were used to calculate reflectivity amplitudes. In the first set (Fig. 3), the velocity and Poisson's ratio is varied for a thin layer of high-velocity hydrate;

immediately above and below the hydrate, velocities are near 1.8 km/s and the Poisson's ratio is 0.46. Model amplitudes match reasonably well with the observed amplitudes for a 7 m thick hydrate layer with Poisson's ratio and velocity 2.1-2.6 km/s. For either thicker layers or larger Poisson's ratios, amplitudes increase less rapidly than the observed data for array offsets of 2 km or less, and more rapidly at the larger offsets. In the second set of models (Fig. 3), a gas-saturated layer with a p-wave velocity of 1.53 km/s and Poisson's ratio of 0.20 is located beneath sediments with velocity 1.9 km/s and Poisson's ratio 0.46. For gas layer thicknesses of 60 m or more, a reflection from the base of the gas layer would also be produced, which is not observed in the data. Subsequently, for all layer thicknesses, the amplitudes increase with offset more rapidly than the measured values.

REFERENCES

Clowes, R.M., Brandon, M.T., Green, A.G., Yorath, C.J., Sutherland Brown, Kanasewich, E.R. and Spencer, C., LITHOPROBE - southern Vancouver Island: Cenozoic subduction complex imaged by deep seismic reflections, *Can. J. Earth Sci., 24*, 31-51, 1987.

Davis, E.E. and Hyndman, R.D., Accretion and recent deformation of sediments along the northern Cascadia subduction zone, *Geol. Soc. Am. Bull., 101*, 1465-1480, 1989.

Davis, E.E., Hyndman, R.D. and Villinger, H., Rates of fluid expulsion across the northern Cascadia Accretionary prism: constraints from new heat flow and multichannel seismic reflection data, *J. Geophys. Res., 95*, 8869-8889, 1990.

Fuchs, K. and Muller, G., Computations of synthetic seismograms with the reflectivity method and comparison with observations, *Geophys. J., 23*, 417-433, 1971.

Green, A.G., Clowes, R.M., Yorath, C.J., Spencer, C., Kanasewich, E.R., Brandon and A. Sutherland Brown, Seismic reflection imaging of the subducting Juan de Fuca plate, *Nature, 319*, 210-213, 1986.

Green, A.G., Milkereit, B., Mayrand, L., Spencer, C., Kurtz, R. and Clowes, R.M., LITHOPROBE seismic reflection profiling across Vancouver Island: results from reprocessing, *Geophys. J., 89*, 85-90, 1987.

Hyndman, R.D., Yorath, C.J., Clowes, R.M. and Davis, E.E., The northern Cascadia subduction zone at Vancouver Island: Structure and tectonic history, *Can. J. Earth Sci., 27*, 313-329, 1990.

Hyndman, R.D. and Davis, E.E., A mechanism for the formation of methane hydrate and sea floor bottom simulating reflectors by vertical fluid expulsion, *J. Geophys. Res.* (in press).

Riddihough, R.P, A model for recent plate interactions of Canada's west coast, *Can. J. Earth Sci., 14*, 384-396, 1977.

Riddihough, R.P., Structure and gravity of an active margin - British Columbia and Washington, *Can. J. Earth Sci., 16,* 350-363, 1979.

Riddihough, R.P. and Hyndman, R.D., Modern plate tectonic regime, in *The Cordilleran Orogen: Canada,* edited by H. Gabrielse and C.J. Yorath, *Geol. Surv. Can., Geology of Canada, 4,* (in press)

Shouldice, D.H., Geology of the western Canadian continental shelf, *Bull. Can. Petr. Geol., 19,* 405-436, 1971.

Shuey, R.T., A simplification of the Zoeppritz equations, *Geophysics, 50,* 609-614, 1985.

Spence, G.D., Clowes, R.M. and Ellis, R.M., Seismic structure across the active subduction zone of western Canada, *J. Geophys. Res., 90,* 6754-6772, 1985.

Spencer, C.A., Asudeh, I. and Cote, T., SEGY-LDS Version 2.0 Format Reference Document, *Geol. Surv. Can.,* 17 pp., 1989.

Taber, J.J. and Smith, S.W., Seismicity and focal mechanisms associated with the subduction of the Juan de Fuca plate beneath the Olympic Peninsula, Washington, *Bull. Seism. Soc. Am., 75,* 1985.

Waldron, D.A., Clowes, R.M. and White, D.J., Seismic structure of a subducting oceanic plate off western Canada, in *Studies of laterally heterogeneous structures using seismic refraction and reflection data,* edited by A.G. Green, *Geol. Surv. Can., Paper 89-13,* 1989.

Yorath, C.J., Marine multichannel seismic reflection, gravity and magnetic profiles - Vancouver Island Margin and Juan de Fuca Ridge, *Geol. Surv. Can., Open File 1661,* 1987.

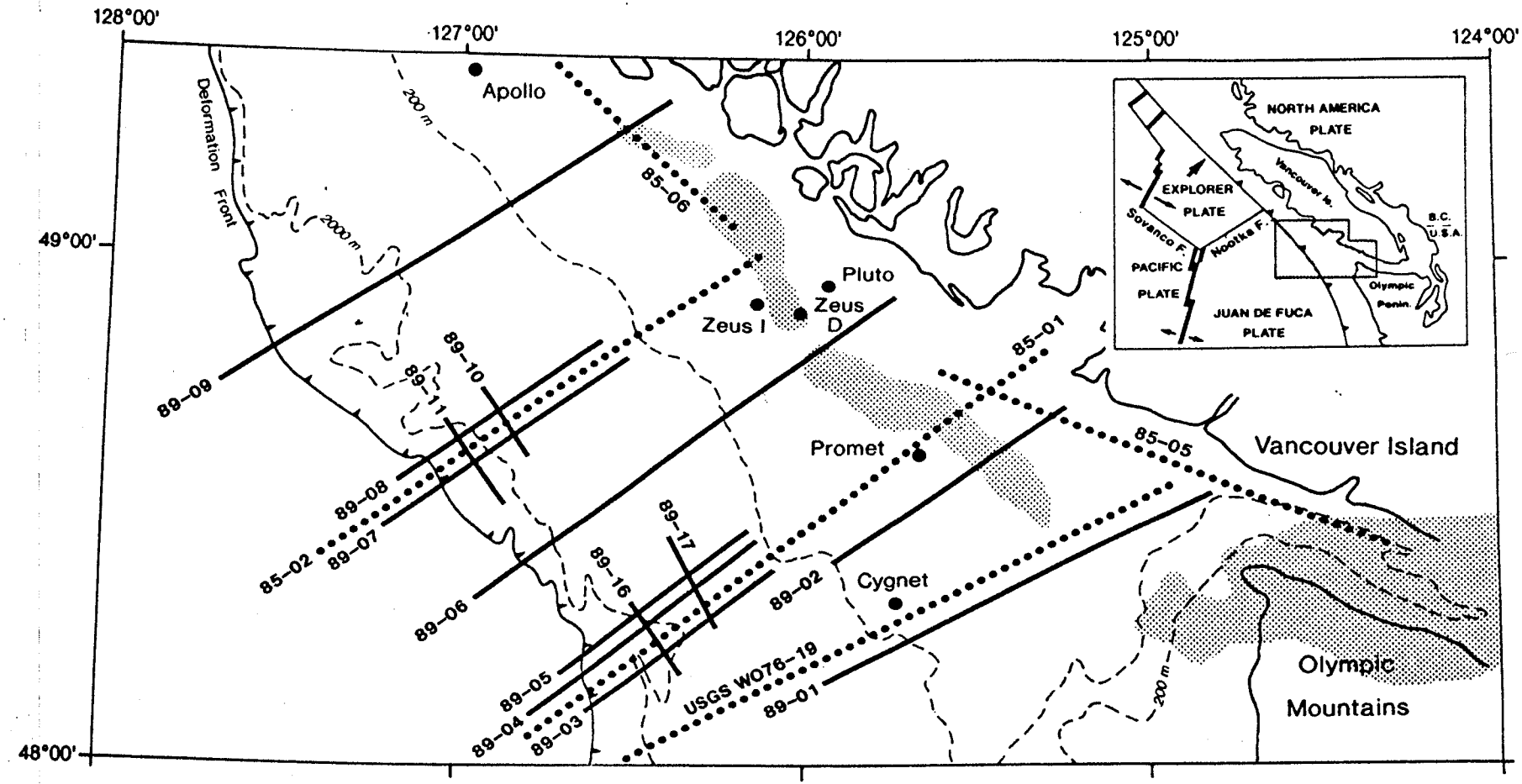

Fig. 1. Location map for the 1989 Cascadia margin multichannel seismic profiles (solid lines; segments shown in Figures 2-4 are indicated by the thickened lines). Locations of older marine multichannel profiles (dotted lines) and offshore exploratory wells are also shown. Hachured areas indicate regions of positive magnetic anomalies on the continental shelf. The shelf edge and lower slope region are defined by the 200 m and 2000 m bathymetry contours.

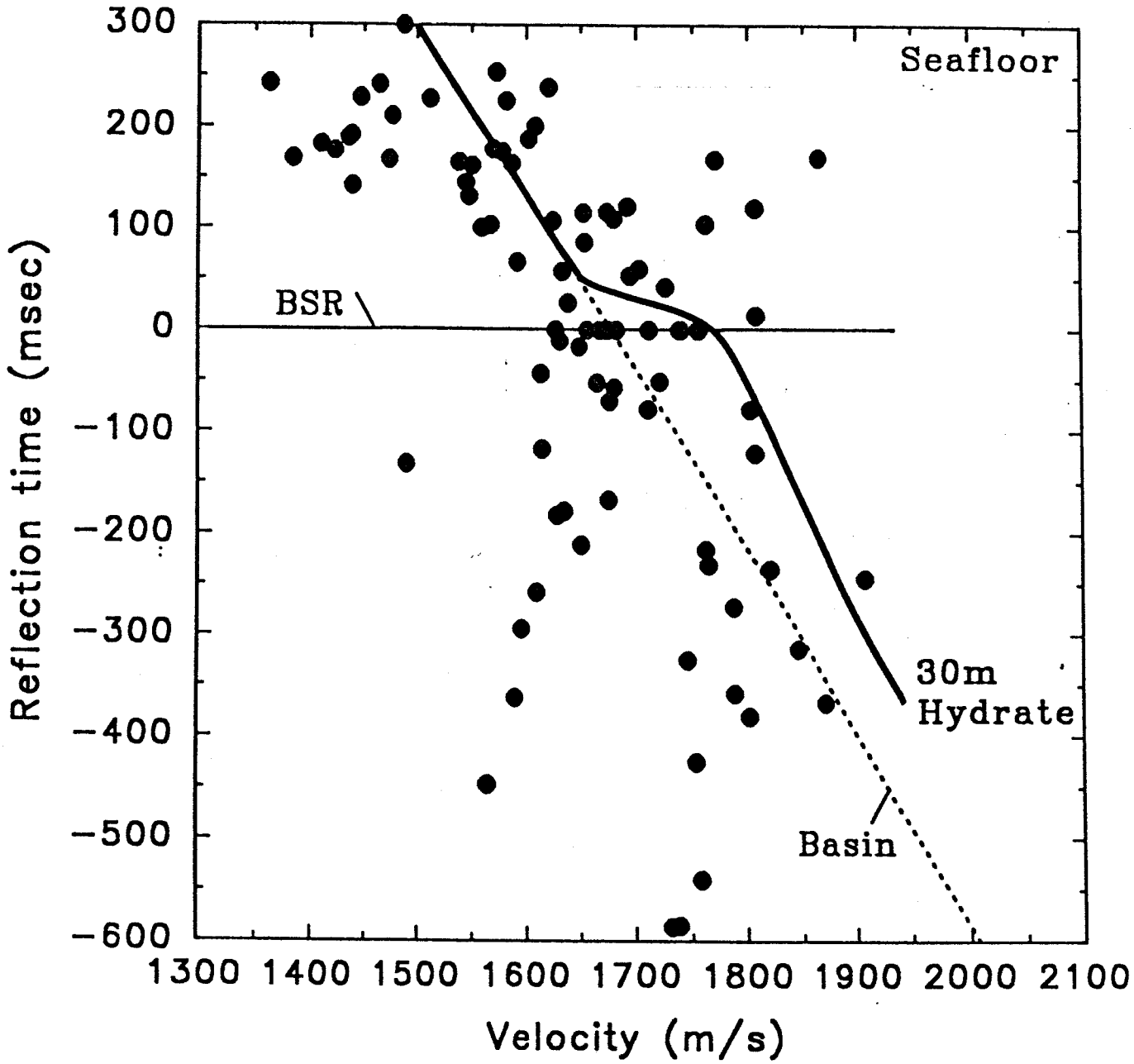
300
200
100
0
−100
−200
−300
−400
−500
−600
Reflection time (msec)
1300 1400 1500 1600 1700 1800 1900 2000 2100
Velocity (m/s)
Seafloor
BSR
30m
Hydrate
Basin

Fig. 2

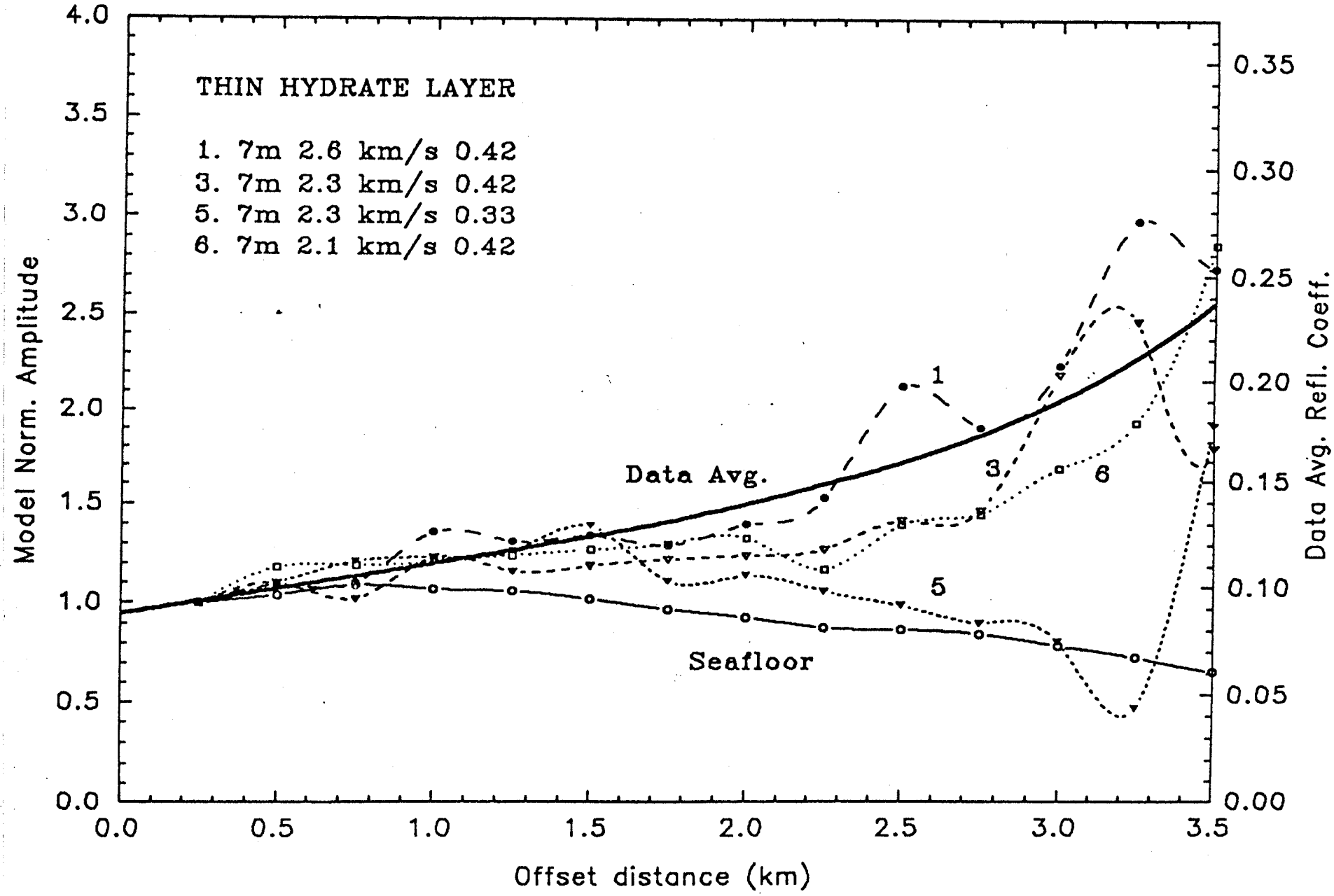

Fig. 3. Variation of amplitude with offset for the bottom simulating reflector. Solid curve shows a highly smoothed set of observed data. Other curves are for a thin high-velocity hydrate layer of variable velocity and Poisson's ratio.

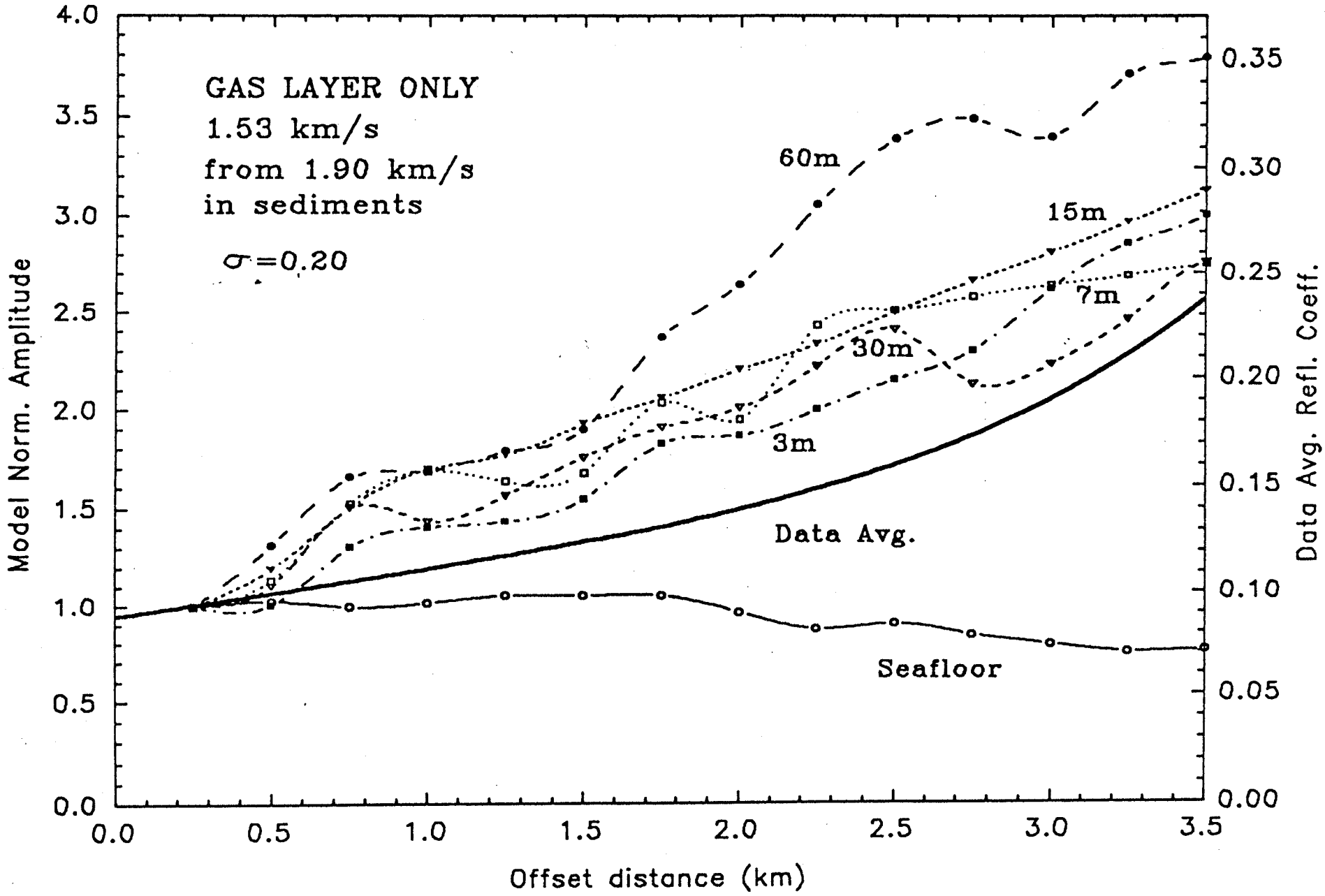

Fig. 4. Variation of amplitude with offset for the BSR. Solid curve is the observed data. Other curves are for a gas-saturated layer of velocity 1.53 km/s and Poisson's ratio 0.20.

APPENDIX 2. Shot point location information.

LINE NUMBER	SHT PNT	LATITUDE	LONGITUDE
89-01	100	48 32 0.4 N	124 49 58.0 W
89-01	150	48 31 24.8 N	124 51 47.5 W
89-01	200	48 30 49.6 N	124 53 37.1 W
89-01	250	48 30 14.0 N	124 55 26.5 W
89-01	300	48 29 38.0 N	124 57 15.6 W
89-01	350	48 29 2.6 N	124 59 5.1 W
89-01	400	48 28 26.9 N	125 0 54.3 W
89-01	450	48 27 51.2 N	125 2 43.6 W
89-01	500	48 27 15.4 N	125 4 32.7 W
89-01	550	48 26 39.8 N	125 6 22.0 W
89-01	600	48 26 4.3 N	125 8 11.3 W
89-01	650	48 25 28.1 N	125 10 0.0 W
89-01	700	48 24 51.5 N	125 11 48.5 W
89-01	750	48 24 15.9 N	125 13 37.7 W
89-01	800	48 23 40.2 N	125 15 26.8 W
89-01	850	48 23 4.7 N	125 17 16.0 W
89-01	900	48 22 28.7 N	125 19 4.8 W
89-01	950	48 21 52.9 N	125 20 53.7 W
89-01	1000	48 21 16.2 N	125 22 42.0 W
89-01	1050	48 20 39.8 N	125 24 30.5 W
89-01	1100	48 20 4.2 N	125 26 19.6 W
89-01	1150	48 19 28.1 N	125 28 8.1 W
89-01	1200	48 18 52.2 N	125 29 56.9 W
89-01	1250	48 18 15.9 N	125 31 45.3 W
89-01	1300	48 17 39.6 N	125 33 33.8 W
89-01	1350	48 17 3.1 N	125 35 22.0 W
89-01	1400	48 16 27.1 N	125 37 10.6 W
89-01	1450	48 15 50.8 N	125 38 59.0 W
89-01	1500	48 15 14.6 N	125 40 47.4 W
89-01	1550	48 14 38.2 N	125 42 35.7 W
89-01	1600	48 14 2.1 N	125 44 24.1 W
89-01	1650	48 13 25.0 N	125 46 11.7 W
89-01	1700	48 12 49.0 N	125 48 0.2 W
89-01	1750	48 12 13.0 N	125 49 48.7 W
89-01	1800	48 11 35.5 N	125 51 36.0 W
89-01	1850	48 10 59.3 N	125 53 24.2 W
89-01	1900	48 10 23.2 N	125 55 12.5 W
89-01	1938	48 9 55.4 N	125 56 34.6 W

TIME FOR START OF LINE	89-01	257	17	41	57
TIME FOR FINISH OF LINE	89-01	258	5	54	47

LINE NUMBER	SHT PNT	LATITUDE	LONGITUDE
89-02	1282	48 41 35.4 N	125 14 56.7 W
89-02	1250	48 41 6.9 N	125 16 1.9 W
89-02	1200	48 40 22.4 N	125 17 44.0 W
89-02	1150	48 39 37.9 N	125 19 26.2 W
89-02	1100	48 38 53.8 N	125 21 8.6 W
89-02	1050	48 38 8.9 N	125 22 50.2 W
89-02	1000	48 37 24.9 N	125 24 32.6 W
89-02	950	48 36 40.4 N	125 26 14.5 W
89-02	900	48 35 55.9 N	125 27 56.4 W
89-02	850	48 35 11.0 N	125 29 38.0 W
89-02	800	48 34 26.3 N	125 31 19.7 W
89-02	750	48 33 42.2 N	125 33 1.9 W
89-02	700	48 32 57.3 N	125 34 43.4 W
89-02	650	48 32 12.4 N	125 36 24.8 W
89-02	600	48 31 28.1 N	125 38 6.7 W
89-02	550	48 30 43.1 N	125 39 48.0 W
89-02	500	48 29 58.1 N	125 41 29.3 W
89-02	451	48 29 14.9 N	125 43 9.4 W

TIME FOR START OF LINE	89-02	254	15 57 16
TIME FOR FINISH OF LINE	89-02	254	21 26 32

LINE NUMBER	SHT PNT	LATITUDE	LONGITUDE
89-02A	492	48 29 51.7 N	125 41 46.2 W
89-02A	450	48 29 14.1 N	125 43 11.4 W
89-02A	400	48 28 29.3 N	125 44 52.7 W
89-02A	350	48 27 43.9 N	125 46 33.5 W
89-02A	300	48 26 59.3 N	125 48 15.1 W
89-02A	250	48 26 14.7 N	125 49 56.5 W
89-02A	200	48 25 30.0 N	125 51 38.0 W
89-02A	150	48 24 44.9 N	125 53 19.0 W
89-02A	100	48 24 0.1 N	125 55 0.3 W

TIME FOR START OF LINE	89-02A	255	2 3 14
TIME FOR FINISH OF LINE	89-02A	255	4 37 32

LINE NUMBER	SHT PNT	LATITUDE	LONGITUDE
89-03	1102	48 23 0.7 N	126 5 28.3 W
89-03	1100	48 22 58.8 N	126 5 32.1 W
89-03	1050	48 22 9.6 N	126 7 8.6 W
89-03	1040	48 21 59.5 N	126 7 27.6 W

TIME FOR START OF LINE 89-03 255 6 26 1
TIME FOR FINISH OF LINE 89-03 255 6 50 29

LINE NUMBER	SHT PNT	LATITUDE	LONGITUDE
89-03A	1081	48 22 40.0 N	126 6 8.6 W
89-03A	1050	48 22 10.0 N	126 7 9.0 W
89-03A	1000	48 21 20.6 N	126 8 45.2 W
89-03A	950	48 20 30.8 N	126 10 21.0 W
89-03A	900	48 19 41.6 N	126 11 57.4 W
89-03A	850	48 18 52.7 N	126 13 33.9 W
89-03A	800	48 18 3.6 N	126 15 10.5 W
89-03A	750	48 17 13.7 N	126 16 45.9 W
89-03A	700	48 16 24.5 N	126 18 22.2 W
89-03A	650	48 15 35.1 N	126 19 58.3 W
89-03A	600	48 14 45.3 N	126 21 33.9 W
89-03A	550	48 13 56.1 N	126 23 10.0 W
89-03A	500	48 13 6.5 N	126 24 45.8 W
89-03A	450	48 12 17.0 N	126 26 21.6 W
89-03A	400	48 11 28.0 N	126 27 57.9 W
89-03A	350	48 10 37.7 N	126 29 32.8 W
89-03A	300	48 9 48.2 N	126 31 8.5 W
89-03A	250	48 8 58.8 N	126 32 44.4 W
89-03A	200	48 8 8.9 N	126 34 19.6 W
89-03A	150	48 7 19.4 N	126 35 55.3 W
89-03A	100	48 6 29.6 N	126 37 30.5 W

TIME FOR START OF LINE 89-03A 255 9 59 00
TIME FOR FINISH OF LINE 89-03A 255 16 9 38

LINE NUMBER	SHT PNT	LATITUDE	LONGITUDE
89-04	100	48 5 59.7 N	126 47 29.7 W
89-04	150	48 6 50.0 N	126 45 54.9 W
89-04	200	48 7 40.2 N	126 44 20.1 W
89-04	250	48 8 29.7 N	126 42 44.5 W
89-04	300	48 9 19.8 N	126 41 9.5 W
89-04	350	48 10 9.4 N	126 39 33.8 W
89-04	400	48 10 59.3 N	126 37 58.5 W
89-04	450	48 11 49.1 N	126 36 23.0 W
89-04	500	48 12 39.0 N	126 34 47.7 W
89-04	550	48 13 28.9 N	126 33 12.4 W
89-04	600	48 14 18.7 N	126 31 36.9 W
89-04	650	48 15 8.3 N	126 30 1.2 W
89-04	700	48 15 57.9 N	126 28 25.3 W
89-04	750	48 16 47.6 N	126 26 49.6 W
89-04	800	48 17 37.4 N	126 25 14.0 W
89-04	850	48 18 26.9 N	126 23 38.0 W
89-04	900	48 19 16.7 N	126 22 2.5 W
89-04	950	48 20 6.8 N	126 20 27.0 W
89-04	1000	48 20 55.9 N	126 18 50.5 W
89-04	1050	48 21 45.6 N	126 17 14.7 W
89-04	1100	48 22 35.3 N	126 15 38.8 W
89-04	1150	48 23 24.4 N	126 14 2.2 W
89-04	1200	48 24 13.9 N	126 12 26.1 W
89-04	1250	48 25 3.6 N	126 10 50.1 W
89-04	1300	48 25 52.9 N	126 9 13.7 W
89-04	1308	48 26 0.8 N	126 8 58.2 W

TIME FOR START OF LINE	89-04	255	19	18	46
TIME FOR FINISH OF LINE	89-04	256	3	32	43

LINE NUMBER	SHT PNT	LATITUDE	LONGITUDE
89-05	1096	48 27 18.2 N	126 10 29.7 W
89-05	1050	48 26 33.0 N	126 11 58.6 W
89-05	1000	48 25 44.1 N	126 13 35.6 W
89-05	950	48 24 55.0 N	126 15 12.2 W
89-05	900	48 24 6.0 N	126 16 49.0 W
89-05	850	48 23 17.6 N	126 18 26.5 W
89-05	800	48 22 28.0 N	126 20 2.5 W
89-05	750	48 21 39.0 N	126 21 39.2 W
89-05	700	48 20 50.3 N	126 23 16.1 W
89-05	650	48 20 1.0 N	126 24 52.4 W
89-05	600	48 19 11.9 N	126 26 28.9 W
89-05	550	48 18 22.9 N	126 28 5.5 W
89-05	500	48 17 33.9 N	126 29 42.0 W
89-05	450	48 16 44.5 N	126 31 18.1 W
89-05	400	48 15 55.0 N	126 32 54.0 W
89-05	350	48 15 5.8 N	126 34 30.3 W
89-05	300	48 14 16.6 N	126 36 6.5 W
89-05	250	48 13 27.4 N	126 37 42.8 W
89-05	200	48 12 38.2 N	126 39 18.8 W
89-05	150	48 11 48.8 N	126 40 54.8 W
89-05	100	48 10 59.1 N	126 42 30.4 W

TIME FOR START OF LINE	89-05	256	6	48	15	
TIME FOR FINISH OF LINE	89-05	256	13	6	9	

LINE NUMBER	SHT PNT	LATITUDE	LONGITUDE
89-06	100	48 19 30.0 N	126 57 0.2 W
89-06	150	48 20 18.7 N	126 55 23.2 W
89-06	200	48 21 7.5 N	126 53 46.3 W
89-06	250	48 21 56.5 N	126 52 9.7 W
89-06	300	48 22 45.0 N	126 50 32.3 W
89-06	350	48 23 33.5 N	126 48 55.2 W
89-06	400	48 24 22.3 N	126 47 18.1 W
89-06	450	48 25 10.6 N	126 45 40.6 W
89-06	500	48 25 59.3 N	126 44 3.5 W
89-06	550	48 26 48.2 N	126 42 26.5 W
89-06	600	48 27 37.0 N	126 40 49.5 W
89-06	650	48 28 25.7 N	126 39 12.3 W
89-06	700	48 29 14.0 N	126 37 34.6 W
89-06	750	48 30 2.3 N	126 35 56.9 W
89-06	800	48 30 51.3 N	126 34 19.9 W
89-06	850	48 31 39.2 N	126 32 41.7 W
89-06	900	48 32 28.0 N	126 31 4.5 W
89-06	950	48 33 16.5 N	126 29 26.9 W
89-06	1000	48 34 4.8 N	126 27 49.0 W
89-06	1050	48 34 53.1 N	126 26 11.2 W
89-06	1100	48 35 41.5 N	126 24 33.3 W
89-06	1150	48 36 29.8 N	126 22 55.5 W
89-06	1200	48 37 18.2 N	126 21 17.6 W
89-06	1250	48 38 6.4 N	126 19 39.5 W
89-06	1300	48 38 54.8 N	126 18 1.7 W
89-06	1350	48 39 43.1 N	126 16 23.6 W
89-06	1400	48 40 31.2 N	126 14 45.4 W
89-06	1450	48 41 19.6 N	126 13 7.4 W
89-06	1500	48 42 7.5 N	126 11 28.8 W
89-06	1550	48 42 55.7 N	126 9 50.6 W
89-06	1600	48 43 44.0 N	126 8 12.5 W
89-06	1650	48 44 32.1 N	126 6 34.1 W
89-06	1700	48 45 16.6 N	126 4 51.7 W
89-06	1750	48 46 0.3 N	126 3 8.3 W
89-06	1800	48 46 48.4 N	126 1 29.9 W
89-06	1850	48 47 36.2 N	125 59 51.0 W
89-06	1900	48 48 24.2 N	125 58 12.4 W
89-06	1950	48 49 12.0 N	125 56 33.5 W
89-06	2000	48 50 0.3 N	125 54 55.1 W
89-06	2050	48 50 48.1 N	125 53 16.1 W
89-06	2100	48 51 36.2 N	125 51 37.5 W
89-06	2150	48 52 23.6 N	125 49 58.0 W
89-06	2200	48 53 11.7 N	125 48 19.4 W
89-06	2250	48 53 59.2 N	125 46 40.0 W
89-06	2300	48 54 47.0 N	125 45 1.0 W
89-06	2316	48 55 2.7 N	125 44 29.6 W

TIME FOR START OF LINE	89-06	253	19	4	37
TIME FOR FINISH OF LINE	89-06	254	10	12	23

LINE NUMBER	SHT PNT	LATITUDE	LONGITUDE
89-07	100	48 27 53.9 N	127 12 41.9 W
89-07	150	48 28 41.1 N	127 11 2.9 W
89-07	200	48 29 28.3 N	127 9 24.0 W
89-07	250	48 30 15.4 N	127 7 45.1 W
89-07	300	48 31 2.1 N	127 6 5.5 W
89-07	350	48 31 49.3 N	127 4 26.5 W
89-07	400	48 32 36.3 N	127 2 47.3 W
89-07	450	48 33 23.2 N	127 1 7.9 W
89-07	500	48 34 10.1 N	126 59 28.6 W
89-07	550	48 34 57.0 N	126 57 49.1 W
89-07	600	48 35 43.8 N	126 56 9.7 W
89-07	650	48 36 30.8 N	126 54 30.4 W
89-07	700	48 37 17.4 N	126 52 50.5 W
89-07	750	48 38 4.4 N	126 51 11.2 W
89-07	800	48 38 51.2 N	126 49 31.4 W
89-07	850	48 39 37.7 N	126 47 51.5 W
89-07	900	48 40 24.6 N	126 46 11.9 W
89-07	950	48 41 11.4 N	126 44 32.2 W
89-07	1000	48 41 58.2 N	126 42 52.4 W
89-07	1050	48 42 44.6 N	126 41 12.2 W
89-07	1100	48 43 31.3 N	126 39 32.4 W
89-07	1150	48 44 18.0 N	126 37 52.4 W
89-07	1200	48 45 4.4 N	126 36 12.2 W
89-07	1250	48 45 50.9 N	126 34 32.0 W
89-07	1300	48 46 37.8 N	126 32 52.3 W
89-07	1350	48 47 24.7 N	126 31 12.4 W
89-07	1353	48 47 28.2 N	126 31 7.1 W

TIME FOR START OF LINE	89-07	252	11	57	11
TIME FOR FINISH OF LINE	89-07	252	19	52	25

LINE NUMBER	SHT PNT	LATITUDE	LONGITUDE
89-08	1104	48 49 35.5 N	126 36 0.2 W
89-08	1100	48 49 31.8 N	126 36 8.4 W
89-08	1050	48 48 44.8 N	126 37 48.0 W
89-08	1000	48 47 57.7 N	126 39 27.7 W
89-08	950	48 47 10.9 N	126 41 7.7 W
89-08	900	48 46 23.4 N	126 42 46.8 W
89-08	850	48 45 36.8 N	126 44 27.0 W
89-08	800	48 44 49.4 N	126 46 6.1 W
89-08	750	48 44 2.3 N	126 47 45.6 W
89-08	700	48 43 15.5 N	126 49 25.3 W
89-08	650	48 42 27.9 N	126 51 4.3 W
89-08	600	48 41 40.7 N	126 52 43.7 W
89-08	550	48 40 53.6 N	126 54 23.2 W
89-08	500	48 40 6.5 N	126 56 2.5 W
89-08	450	48 39 19.1 N	126 57 41.5 W
89-08	400	48 38 31.6 N	126 59 20.4 W
89-08	350	48 37 44.4 N	127 0 59.7 W
89-08	300	48 36 56.6 N	127 2 38.0 W
89-08	250	48 36 9.5 N	127 4 17.4 W
89-08	200	48 35 21.8 N	127 5 55.9 W
89-08	150	48 34 34.3 N	127 7 34.7 W
89-08	100	48 33 47.2 N	127 9 13.9 W
89-08	59	48 33 8.1 N	127 10 34.6 W

TIME FOR START OF LINE	89-08	252	21 29 40
TIME FOR FINISH OF LINE	89-08	253	4 15 39

LINE NUMBER	SHT PNT	LATITUDE	LONGITUDE
89-09A	2305	49 17 59.8 N	126 23 59.5 W
89-09A	2300	49 17 55.5 N	126 24 9.9 W
89-09A	2250	49 17 11.8 N	126 25 54.2 W
89-09A	2200	49 16 27.6 N	126 27 37.7 W
89-09A	2150	49 15 42.3 N	126 29 20.3 W
89-09A	2100	49 14 59.1 N	126 31 4.9 W
89-09A	2050	49 14 15.1 N	126 32 48.5 W
89-09A	2000	49 13 30.3 N	126 34 31.4 W
89-09A	1950	49 12 45.5 N	126 36 14.3 W
89-09A	1900	49 12 1.3 N	126 37 57.8 W
89-09A	1850	49 11 17.0 N	126 39 41.1 W
89-09A	1800	49 10 30.3 N	126 41 22.0 W
89-09A	1750	49 9 48.2 N	126 43 7.5 W
89-09A	1700	49 9 4.0 N	126 44 50.9 W
89-09A	1650	49 8 19.0 N	126 46 33.4 W
89-09A	1600	49 7 34.6 N	126 48 16.5 W
89-09A	1570	49 7 7.8 N	126 49 18.2 W

TIME FOR START OF LINE 89-09A 251 8 20 25
TIME FOR FINISH OF LINE 89-09A 251 12 47 31

LINE NUMBER	SHT PNT	LATITUDE	LONGITUDE
89-09B A	1620	49 7 52.8 N	126 47 35.8 W
89-09B A	1600	49 7 34.4 N	126 48 16.3 W
89-09B	1550	49 6 50.3 N	126 49 59.8 W
89-09B	1500	49 6 5.8 N	126 51 42.8 W
89-09B	1450	49 5 21.4 N	126 53 25.8 W
89-09B	1400	49 4 36.4 N	126 55 8.1 W
89-09B	1350	49 3 51.8 N	126 56 51.0 W
89-09B	1300	49 3 7.8 N	126 58 34.3 W
89-09B	1250	49 2 22.1 N	127 0 15.9 W
89-09B	1200	49 1 37.2 N	127 1 58.3 W
89-09B	1150	49 0 52.4 N	127 3 40.7 W
89-09B	1100	49 0 7.9 N	127 5 23.5 W
89-09B	1050	48 59 22.9 N	127 7 5.9 W
89-09B	1000	48 58 38.2 N	127 8 48.3 W
89-09B	950	48 57 53.3 N	127 10 30.6 W
89-09B	900	48 57 8.5 N	127 12 13.0 W
89-09B	850	48 56 23.6 N	127 13 55.2 W
89-09B	800	48 55 37.8 N	127 15 36.5 W
89-09B	750	48 54 53.5 N	127 17 19.3 W
89-09B	700	48 54 8.5 N	127 19 1.3 W
89-09B	650	48 53 23.6 N	127 20 43.3 W
89-09B	600	48 52 38.8 N	127 22 25.6 W
89-09B	550	48 51 53.6 N	127 24 7.3 W
89-09B	500	48 51 8.5 N	127 25 49.2 W
89-09B	450	48 50 23.5 N	127 27 31.1 W
89-09B	400	48 49 38.0 N	127 29 12.5 W
89-09B	350	48 48 52.9 N	127 30 54.2 W
89-09B	300	48 48 8.1 N	127 32 36.3 W
89-09B	250	48 47 22.6 N	127 34 17.6 W

89-09B	200	48 46 37.5 N	127 35 59.3 W
89-09B	150	48 45 52.4 N	127 37 41.0 W
89-09B	100	48 45 6.7 N	127 39 22.0 W
89-09B	59	48 44 29.6 N	127 40 45.2 W

TIME FOR START OF LINE 89-09B 251 19 30 57
TIME FOR FINISH OF LINE 89-09B 252 6 48 34

LINE NUMBER	SHT PNT	LATITUDE	LONGITUDE
89-10	397	48 36 29.2 N	126 47 58.3 W
89-10	350	48 37 30.9 N	126 49 5.6 W
89-10	300	48 38 36.7 N	126 50 16.6 W
89-10	250	48 39 42.7 N	126 51 27.3 W
89-10	200	48 40 48.7 N	126 52 38.0 W
89-10	150	48 41 54.4 N	126 53 49.4 W
89-10	100	48 43 0.5 N	126 55 0.0 W
89-10	59	48 43 54.5 N	126 55 58.4 W

TIME FOR START OF LINE 89-10 253 8 39 36
TIME FOR FINISH OF LINE 89-10 253 10 45 19

LINE NUMBER	SHT PNT	LATITUDE	LONGITUDE
89-11	100	48 40 0.0 N	127 2 0.0 W
89-11	150	48 38 54.3 N	127 0 48.8 W
89-11	200	48 37 48.4 N	126 59 38.0 W
89-11	250	48 36 42.6 N	126 58 26.9 W
89-11	300	48 35 36.6 N	126 57 16.2 W
89-11	350	48 34 30.9 N	126 56 5.0 W
89-11	400	48 33 24.8 N	126 54 54.7 W
89-11	438	48 32 34.7 N	126 54 0.7 W

TIME FOR START OF LINE 89-11 253 13 8 4
TIME FOR FINISH OF LINE 89-11 253 15 13 58

LINE NUMBER	SHT PNT	LATITUDE	LONGITUDE
89-12	100	48 31 17.3 N	128 53 36.2 W
89-12	150	48 30 56.6 N	128 51 38.4 W
89-12	200	48 30 34.9 N	128 49 41.0 W
89-12	250	48 30 13.4 N	128 47 43.6 W
89-12	300	48 29 52.1 N	128 45 46.1 W
89-12	350	48 29 31.3 N	128 43 48.5 W
89-12	400	48 29 10.7 N	128 41 50.7 W
89-12	450	48 28 50.1 N	128 39 53.0 W
89-12	500	48 28 29.8 N	128 37 55.0 W
89-12	550	48 28 9.6 N	128 35 57.2 W
89-12	600	48 27 48.8 N	128 33 59.6 W
89-12	604	48 27 47.2 N	128 33 50.2 W

TIME FOR START OF LINE 89-12 286 6 50 25
TIME FOR FINISH OF LINE 89-12 286 9 57 30

LINE NUMBER	SHT PNT	LATITUDE	LONGITUDE
89-13	1002	48 25 53.7 N	128 34 48.1 W
89-13	1000	48 25 54.7 N	128 34 52.8 W
89-13	950	48 26 17.1 N	128 36 49.7 W
89-13	900	48 26 40.5 N	128 38 46.1 W
89-13	850	48 27 3.3 N	128 40 42.9 W
89-13	800	48 27 26.0 N	128 42 39.6 W
89-13	750	48 27 47.6 N	128 44 36.9 W
89-13	700	48 28 9.5 N	128 46 34.1 W
89-13	650	48 28 30.3 N	128 48 31.7 W
89-13	600	48 28 52.1 N	128 50 28.9 W
89-13	550	48 29 13.3 N	128 52 26.4 W
89-13	500	48 29 34.7 N	128 54 23.8 W
89-13	450	48 29 56.1 N	128 56 21.3 W
89-13	400	48 30 17.2 N	128 58 18.9 W
89-13	350	48 30 38.3 N	129 0 16.4 W
89-13	300	48 30 60.0 N	129 2 13.9 W
89-13	250	48 31 21.1 N	129 4 11.4 W
89-13	200	48 31 42.0 N	129 6 9.3 W
89-13	150	48 32 3.5 N	129 8 6.6 W
89-13	100	48 32 24.9 N	129 10 4.2 W

TIME FOR START OF LINE 89-13 285 22 11 20
TIME FOR FINISH OF LINE 89-13 286 4 0 58

LINE NUMBER	SHT PNT	LATITUDE	LONGITUDE
89-14	604	48 24 59.7 N	128 35 5.7 W
89-14	600	48 25 1.4 N	128 35 15.0 W
89-14	550	48 25 24.9 N	128 37 11.4 W
89-14	500	48 25 48.6 N	128 39 7.7 W
89-14	450	48 26 10.9 N	128 41 4.6 W
89-14	400	48 26 31.6 N	128 43 2.1 W
89-14	350	48 26 51.1 N	128 45 0.3 W
89-14	300	48 27 11.0 N	128 46 58.2 W
89-14	250	48 27 31.1 N	128 48 56.1 W
89-14	200	48 27 50.5 N	128 50 54.3 W
89-14	150	48 28 10.7 N	128 52 52.1 W
89-14	100	48 28 30.1 N	128 54 50.2 W

TIME FOR START OF LINE 89-14 286 12 23 2
TIME FOR FINISH OF LINE 89-14 286 15 55 13

LINE NUMBER	SHT PNT	LATITUDE	LONGITUDE
89-15	100	47 55 0.4 N	128 41 60.0 W
89-15	150	47 54 38.4 N	128 40 4.1 W
89-15	200	47 54 17.4 N	128 38 7.7 W
89-15	250	47 53 56.0 N	128 36 11.7 W
89-15	300	47 53 34.4 N	128 34 15.7 W
89-15	350	47 53 13.2 N	128 32 19.6 W
89-15	400	47 52 51.6 N	128 30 23.6 W
89-15	450	47 52 30.2 N	128 28 27.5 W
89-15	500	47 52 8.6 N	128 26 31.6 W
89-15	550	47 51 46.9 N	128 24 35.7 W
89-15	600	47 51 25.3 N	128 22 39.8 W
89-15	650	47 51 3.6 N	128 20 43.9 W
89-15	700	47 50 42.2 N	128 18 48.1 W
89-15	750	47 50 20.3 N	128 16 52.3 W
89-15	800	47 49 58.6 N	128 14 56.4 W
89-15	850	47 49 37.0 N	128 13 0.6 W
89-15	900	47 49 15.2 N	128 11 4.8 W
89-15	950	47 48 53.0 N	128 9 9.2 W
89-15	1000	47 48 31.1 N	128 7 13.6 W
89-15	1050	47 48 9.6 N	128 5 17.7 W
89-15	1100	47 47 47.3 N	128 3 22.3 W
89-15	1150	47 47 25.9 N	128 1 26.4 W
89-15	1200	47 47 3.4 N	127 59 30.9 W
89-15	1250	47 46 41.6 N	127 57 35.3 W
89-15	1300	47 46 19.3 N	127 55 39.9 W
89-15	1350	47 45 57.1 N	127 53 44.4 W
89-15	1400	47 45 35.0 N	127 51 48.9 W
89-15	1450	47 45 13.2 N	127 49 53.4 W
89-15	1500	47 44 50.9 N	127 47 57.9 W
89-15	1550	47 44 28.7 N	127 46 2.5 W
89-15	1600	47 44 6.9 N	127 44 7.0 W
89-15	1650	47 43 44.2 N	127 42 11.8 W
89-15	1700	47 43 22.4 N	127 40 16.2 W
89-15	1750	47 42 59.7 N	127 38 21.1 W
89-15	1800	47 42 37.0 N	127 36 26.0 W
89-15	1850	47 42 15.2 N	127 34 30.5 W
89-15	1900	47 41 52.6 N	127 32 35.3 W
89-15	1950	47 41 29.5 N	127 30 40.5 W
89-15	2000	47 41 7.2 N	127 28 45.2 W
89-15	2050	47 40 45.0 N	127 26 49.9 W
89-15	2100	47 40 22.3 N	127 24 54.8 W
89-15	2150	47 39 59.7 N	127 22 59.8 W
89-15	2187	47 39 42.8 N	127 21 34.8 W

TIME FOR START OF LINE	89-15	287	2 41 49
TIME FOR FINISH OF LINE	89-15	287	15 43 7

LINE NUMBER	SHT PNT	LATITUDE	LONGITUDE
89-16	100	48 18 48.0 N	126 29 47.6 W
89-16	150	48 17 40.3 N	126 28 41.2 W
89-16	200	48 16 32.9 N	126 27 34.1 W
89-16	250	48 15 25.2 N	126 26 27.6 W
89-16	300	48 14 17.6 N	126 25 21.0 W
89-16	350	48 13 10.0 N	126 24 14.2 W
89-16	425	48 11 28.7 N	126 22 34.0 W

TIME FOR START OF LINE	89-16	256	17	14	50
TIME FOR FINISH OF LINE	89-16	256	19	28	29

LINE NUMBER	SHT PNT	LATITUDE	LONGITUDE
89-17	483	48 16 5.4 N	126 14 46.9 W
89-17	450	48 16 52.6 N	126 15 24.3 W
89-17	400	48 18 4.2 N	126 16 20.9 W
89-17	350	48 19 15.7 N	126 17 17.7 W
89-17	300	48 20 27.5 N	126 18 13.8 W
89-17	250	48 21 39.0 N	126 19 10.8 W
89-17	200	48 22 50.5 N	126 20 7.7 W
89-17	150	48 24 2.0 N	126 21 4.6 W
89-17	100	48 25 13.3 N	126 22 2.1 W
89-17	39	48 26 40.5 N	126 23 11.7 W

TIME FOR START OF LINE	89-17	256	21	35	9
TIME FOR FINISH OF LINE	89-17	257	0	42	5

SEISMIC STRUCTURE OF THE NORTHERN CASCADIA ACCRETIONARY PRISM: EVIDENCE FROM NEW MULTICHANNEL SEISMIC REFLECTION DATA

G.D. Spence

Department of Physics and Astronomy
and Centre for Earth and Ocean Research
University of Victoria, Victoria, B.C., Canada V8W 3P6

R.D. Hyndman, E.E. Davis and C.J. Yorath

Pacific Geoscience Centre
Geological Survey of Canada, Sidney, B.C., Canada V8L 4B2

Abstract. Within the Cascadia accretionary prism west of Vancouver Island, new marine seismic reflection profiles totalling 722 km provide improved images which enable the three-dimensional variation of structures along the margin to be determined. At the deformation front, landward dipping thrusts spaced roughly 5 km apart are commonly observed which may penetrate to near the top of the subducting oceanic crust. Along lines separated by 3 km, the amount of displacement on a given fault is seen to vary significantly along the margin. Seaward dipping faults occasionally develop, propagating upward from the frontal thrust. In one region above gently-dipping oceanic crust, a shallow taper sediment wedge has formed, implying high pore fluid pressures along the detachment surface at the top of the oceanic crust. The detachment exhibits a strong reflection probably indicative of high fluid pressure. The accretionary prism is bounded by a landward dipping continental backstop, formed by the marine volcanic Crescent Terrane. The base of this terrane is imaged extending down to near the top of the subducting oceanic crust, so that little sediment is available for deeper subduction or underplating. The seaward part of the Crescent Terrane appears to have been uplifted, probably as a response to the accretion of prism sediments.

Introduction

The western Canadian convergent margin, where the Juan de Fuca plate subducts beneath the North America plate, has been the subject of numerous recent geophysical and geological studies. Hyndman et al. [1990] present a summary of the recent onshore and offshore regional geophysical work, which includes multichannel seismic reflection, shallow seismic profiling, seismic refraction, gravity and magnetic surveys, plus geothermal, seismicity and magnetotelluric measurements.

As part of the first phase of the multidisciplinary Canadian LITHOPROBE program in 1984, high-quality multichannel reflection data were collected across Vancouver Island [Clowes et al., 1987; Green et al., 1986, 1987]. In 1985, widely spaced offshore multichannel seismic lines were recorded across the continental shelf and slope, as part of the Frontier Geoscience Program of the Geological Survey of Canada. Integrated with the previous geophysical and geological data, the main results

of this offshore program [Hyndman et al., 1990; Davis and Hyndman, 1989; Davis et al., 1990; Hyndman and Davis, 1991] were

(1) the definition of landward dipping thrusts at the deformation front which cut through the sediment section to near the igneous ocean crust basement, implying that few sediments are available for underplating or deep subduction.

(2) the delineation of two narrow terranes accreted to the margin in the Eocene (about 42 Ma) - the Mesozoic marine sedimentary Pacific Rim Terrane and the Eocene marine volcanic Crescent Terrane.

(3) the imaging of the top of the downgoing oceanic crust to depths of over 40 km beneath Vancouver Island.

(4) the recognition that the shallow "bottom-simulating-reflector" observed beneath the lower continental slope marked the base of a layer of methane hydrate that could be used as a measure of temperature gradient and heat flow. Subsequently, it has been suggested that the hydrate layer can be used as a semi-quantitative indicator of fluid flow from within the accretionary prism.

In this paper we present new seismic data that provide additional constraints on the structure and tectonic processes in the region. As part of site surveys for the international Ocean Drilling Program, 722 km of marine multichannel reflection lines were collected in 1989 across the western Canadian convergent margin (Figure 1). The primary objective of the program was to determine the three-dimensional variation of structures along the Vancouver Island subduction zone. Of particular interest were the geometry of the accretionary wedge and the accreted terranes, the variation in thrust and fold structures at the deformation front, the nature of the basal thrust or detachment that could produce very large earthquakes, and characteristics of the bottom simulating reflector. This paper presents a preliminary description and interpretation of some of the prominent features on the record sections.

Data Acquisition and Processing

Four of the new lines crossed the continental shelf (lines 1, 2, 6, 9; see Figure 1). These were also recorded by the University of British Columbia at two or more land refraction sites near the end of each line, to provide important deep velocity information. Detailed grids of lines, at approximately 3 km spacing, were recorded across the deformation front in two regions covering sites proposed for scientific drilling by the Ocean Drilling Program. Three new profiles (lines 3, 4, 5) were run parallel to the 1985 Line 1, the extension of the main Lithoprobe land seismic line, and two profiles (lines 7, 8) were obtained parallel to the 1985 Line 2. As well, two cross lines were collected in each region.

The airgun array source had a total volume of 125 L (7820 in^3). A 144-channel streamer recorded 36-fold data to a maximum offset of 3795 m. The shot and group intervals were 50 m and 25 m, respectively. Shots were fired by an integrated navigation system controlled by Starfix.

Processing procedures included (1) true amplitude recovery, with the application of exponential gain and spherical divergence corrections; (2) f-k velocity filter to suppress low velocity backscatter; (3) zero-phase source designature plus f-k demultiple; (4) derivation of stacking velocities from semblance analyses for sub-bottom times less than about 5 s, combined with a general refraction velocity model for the area for greater depths [Waldron et al., 1989]; (5) gapped deconvolution after

stacking; (6) f-k migration, using hand-smoothed NMO functions with 10% velocity reduction to prevent over-migration.

Preliminary Interpretation

Structures Near the Deformation Front

(i) Frontal folds and faults. Figure 2 shows the seaward portion of Lines 3 and 4. The sediment sequence incoming from Cascadia Basin comprises a rapidly-deposited Pleistocene turbidite section (upper 1.5 s) overlying a finer-grained pre-Pleistocene hemipelagic unit (lower 0.8 s). At the deformation front, the sediment section is folded and faulted into margin-parallel anticlinal ridges with the steeper limbs facing seaward [Davis and Hyndman, 1989]. Thrust faults and related anticlines occur at a spacing of about 5 km (LDF in Figure 2) and in some cases appear to penetrate almost completely through the sediment section. Thrust faults are defined both by relative reflector displacements across the fault, and by reflections from the fault plane itself. Asymmetrical anticlines in the fault hanging wall develop as material moves up the thrust ramp; the steep seaward-facing slope is formed landward of where the thrust breaks the surface or flattens near the seafloor. A gently landward-dipping limb develops as the sediment package in the hanging wall is rotated. The uplift of the hanging wall strata can be used to constrain the profile of the thrusts. In some cases the layers are backtilted in a highly planar fashion which requires the thrusts to be circular in profile [Davis and Hyndman, 1989].

The four profiles 89-03, 85-01, 89-04 and 89-05 in the southeastern detailed area (Figure 1) have separations of only 3 km, so the three-dimensional variation of deformation along the margin can be determined. For a given line, the offsets of reflective turbidite horizons are used to calculate displacements along the thrusts. The velocity at the depth of a given horizon is estimated from reflection velocity analyses [Davis et al., 1990, Figure 9], and the local dip of the thrust ramp determined. Near the base of the turbidites, dips range from 30° to 40°. The vertical uplift of the thrust packet is measured, and displacements along the faults are calculated by simple trigonometry. At this time only a single value has been determined for each fault, although the data quality will probably permit the variation in displacement with depth to be resolved.

From Table 1, a systematic variation along strike is seen for the four lines. Displacements along the most seaward fault LDF1 increase substantially to the north from about 300 m on Line 89-03 to 100 m on Line 89-05, while displacements along LDF2 decrease slightly to the north from 1150 m to 950 m. The more landward fault LDF3 is not clearly identified on Line 89-03, but on the other 3 lines there is a northerly increase in fault displacement to over 300 m for Line 89-05.

On the frontal thrust of Line 89-03 (LDF1 in Figure 3), the shallowest sediments above the thrust at SP 250 are undisturbed. A similar relationship is seen on Line 85-01 [Davis and Hyndman, 1989]. One explanation for this is that the fault is simply in the process of propagating upwards, and has not yet broken the surface. Deformation at an even earlier stage than LDF1 is possibly present over the region 1-2 km farther seaward on Line 89-03, where some indications are seen of small fault displacements and folding. The presence of a proto-thrust zone has also

been observed on the Nankai margin [Moore et al., 1990] and the Chile margin [R. von Huene, pers. comm., 1991], and small-displacement thrusts in the early stages of upward propagation are noted at the deformation front off Mexico [Moore and Shipley, 1988]. An alternative explanation for the undisturbed near-surface sediments on Line 89-03 is that the motion on the fault has ceased, and thus the most recent activity does not necessarily occur on the seaward-most fault [Davis and Hyndman, 1989]. Although beyond the scope of this preliminary paper, a thorough analysis is required of the variation in fault displacement with depth and the deformation above the fault termination.

A seaward-dipping backthrust SDF has developed on Line 89-03 (Figure 2, SP 300-330). On the Oregon margin, similiar subsidiary backthrusts propagate upward from the frontal thrust, and seaward-dipping primary thrusts also occur [MacKay et al., 1989]. On the Vancouver Island margin, other seaward dipping thrusts are observed on the northernmost Line 9 (Figure 3), where a major fault approaches the seafloor near SP 430, and on 1985 Line 85-04. Davis and Hyndman [1989] noted deformation through the entire sediment section of the latter line, on two seaward dipping thrust faults located 10-15 km landward of the main frontal anticline.

On Line 89-03, the seaward-dipping fault is symmetric in profile to the landward-dipping frontal thrust from which it appears to have initiated. The two faults form a conjugate pair with a central block of upward displaced sediments. On Line 89-04 (Figure 2) and Line 89-05, the seaward-dipping fault is not seen, but the upper beds, which a maintain a near-horizontal attitude, are vertically uplifted even more than on Line 89-03 (Table 1). At the landward boundary of the central block of sediments on the former two lines, deformation is accomplished by folding instead of faulting. The different deformation mechanisms imply that there is along-strike variability in the mechanical strength of the sediments. If pore-fluid pressure is the key factor in controlling material strength, then the localized variations in the style of deformation imply that there may be localized variations of pore-fluid pressure.

(ii) Location of the décollement. For two-way times of more than 0.5-1.0 s beneath the seafloor, the dips on most of the main thrust faults decrease with depth. When the thrust penetrates to within the lower hemipelagic unit, it is difficult to identify unambiguously the décollement where the thrust soles out. The difficulty arises because of the small vertical offsets expected at low angles and because of the small number of reflection horizons in the hemipelagic sediments. As well, there is difficulty in locating the top of oceanic crust because reflections in the region of the basement are typically low frequency with a period of 100-150 ms, leading to an uncertainty in location of 200 m or more.

Davis and Hyndman [1989] present indirect arguments that the décollement on the Cascadia margin soles out near the top of the oceanic crust, and with the new multichannel seismic data the arguments appear to remain valid. First, as dicussed above, the backtilting of sediment horizons in the hanging wall define the thrust profile. In the special case of a circular profile, the rearward limit of tilting defines the intersection point between the thrust and the basal detachment. As on Line 85-01, tilting on Line 89-03 (Figure 2) extends at least 8 km landward of the main thrust LDF2, at which point an extrapolated circular fault profile is

close to the level of the oceanic basement. The second line of evidence is the sediment budget. As calculated by Davis and Hyndman [1989], the volume of material within the wedge is comparable to the volume of material that has entered the subduction zone, implying that most of the sediments have been off-scraped and accreted.

Other lines, for which deformation is on a horizontal scale of 5 km or less, do not provide as reliable an estimate for the location of the décollement. Definition of the thrust plane often becomes ambiguous within 0.5 s (~700 m) or more above the basement. In a restricted sense, the conclusion that thrusts penetrate close to basement applies only to the second thrust LDF2; for the frontal thrust LDF1 the detachment level may be as high as the middle of the hemipelagic sediment section. The décollement may then step down landwards, as has been noted for the Nankai margin [Moore et al., 1990], the Aleutian margin [McCarthy and Scholl, 1985] and the Barbados margin [Westbrook and Smith, 1983]. This then provides the mechanism allowing underthrusting sediment to be underplated to the accretionary prism.

In many subduction zones the décollement clearly lies within the sediments for significant distances landward of the deformation front. Subducted sediments are traced for 5-7 km from the toe of the Middle America Trench [Moore et al., 1988], at least 20 km in front of the Aleutian subduction zone [McCarthy and Scholl, 1985], about 30 km landward of the Nankai Trench [Moore et al., 1990], and up to 74 km from the edge of the Barbados Accretionary Complex [Westbrook and Smith, 1983].

(iii) Anomalously thin wedge taper, Line 9. The deformation along Line 9 (Figure 3) provides insight into some of the basic principles involved in the formation of a basal detachment and accretionary wedge critical taper [e.g. Davis et al., 1983]. Landward of the frontal anticline, the water depth is nearly constant for almost 30 km; bathymetry charts show a lobe-like region of uniform water depth. On the seismic section, the top of the ocean crust can be followed clearly for 35 km landward of the deformation front with a very small dip (about 3°). Thus, the sediment wedge here has an unusually small taper. According to critical wedge theory, such a shallow taper must be associated with extemely low shear strength of the basal décollement. The main factor controlling sediment strength is taken to be pore pressure, so that very high pore fluid pressure is needed for the detachment surface at the oceanic crust to run far seaward and for the overlying wedge to maintain such a low taper angle. The presence of prominent reflections near the basement below the deformation front (SP 300 to SP 500 near 5 s) corroborates this interpretation. The reflections, which exhibit strong continuity and high apparent amplitudes, could be produced at the top of a detachment zone in the sediments just above the basement, where sediment velocities decrease sharply due to the elevated pore pressures [Calvert and Clowes, 1990; Moore et al., 1990]. This will be studied by further true-amplitude analysis, to determine if the reflections have reverse polarity as expected for a velocity decrease and to see if the interface exhibits the appropriate amplitude variation with incident angle.

On Line 9 the entire thrust package exhibits extensive deformation involving both faulting and folding. Landward of the frontal anticline, there is evidence for additional seaward dipping faults (e.g. SP 550) and

broad folds (e.g. as shown in the blowup of Figure 3), which are similar to structures at the current deformation front on Line 9. Folding at some locations in the upper sediments suggests that there may have been recent deformation within the thrust sheet. For example, intense short-wavelength synclinal folding occurs above 4 s at two locations (SP 550 and SP 630), while broad folds between SP 800 and SP 900 show deformation at depths greater than 100-200 ms below the seafloor. The implication is that the upper portion of the thrust sheet has sufficient strength to transmit stresses up to 30 km from the deformation front, which could be due to either pore pressure effects or to lithology. The upper section comprises turbities and so is coarser than the underlying hemipelagic sediments; the deeper part of the section should thus sustain higher pore pressures and possess less cohesion.

Structure Beneath the Continental Shelf

The four new seismic lines across the continental shelf provide improved images showing the relationship between the accretionary sedimentary wedge and the overlying terranes which now form part of the continental framework. Of particular importance, a reflector that may mark the Crescent thrust or lower boundary of the igneous Crescent Terrane can be traced down to 6.5 s at SP 1950 on Line 6 (Figure 4). The terrane acts as the landward dipping backstop to the accretionary prism. This depth is very close to the top of the subducting oceanic crust. Thus, if this interpretation is correct, very few sediments are available for deeper subduction or continental underplating.

At the base of the accretionary prism on Line 6, very bright nearly horizontal reflections are seen near 6 s between SP 1400 and SP 1700. The reflections are located at the approximate depth expected for the top of the oceanic crust beneath the outer continental shelf. However, because of their high amplitude and smooth character, they are unlikely to arise directly from the lithological contrast between the accreted sediments and the rough surface of the dipping oceanic crust. The impedance contrast producing the reflections may arise from a shear zone containing high-pressure fluids. In a subduction zone environment, high strains exist and fluid-rich sediments are present, perhaps trapped between the overlying backstop and the oceanic crust.

The Crescent Terrane comprises Eocene oceanic basalts which have been penetrated by exploratory wells in Tofino Basin [Shouldice, 1971] and which are exposed on southern Vancouver Island and the Olympic Peninsula. Its location beneath the shelf is marked by a magnetic high [Hyndman et al., 1990] which can be traced parallel to the margin for over 150 km (Figure 1). The position of the magnetic high corresponds well with the location of the Crescent Terrane determined from the seismic profile (Figure 4). The Crescent material appears to extend somewhat farther seaward than the magnetic high, but the thickness of these rocks may be small at their seaward edge. In contrast, the main body of the Crescent Terrane appears to have a thickness of 3.5 s or more (i.e. about 10 km). The section may have been thickened by imbrication such as is observed on land within the Crescent volcanics [Massey, 1986].

Further information on the mechanism of emplacement of the Crescent Terrane is revealed by the new seismic data. As discussed by Hyndman et al. [1990], one model of emplacement proposes that the subduction

zone stepped seaward after the complete oceanic lithosphere was faulted and underthrust, while in a second model a sliver of oceanic crust was detached from the top of the subducting plate. The new seismic lines show evidence for uplift of the seaward portion of the Crescent Terrane, perhaps associated with thrusting of accretionary wedge sediments. As typified by Line 6 (Figure 4), most dips within the terrane are landward, and a basement ridge at SP 1800 separates Tofino Basin into two sections. On Line 2 (not shown) at the base of the landward section, the onlap pattern of sediments at the top surface of the Crescent Terrane clearly indicates a pattern of uplift in the west relative to the east. An equivalent pattern is not seen at the base of the Tofino Basin section seaward of the basement ridge. Thus, uplift or tilting since the initiation of sediment deposition has probably occured by imbrication or duplexing within the Crescent Terrane itself.

Conclusions

With the improved images from our new seismic data, the three-dimensional variation of deformation along the margin can be determined. Although it is often difficult to determine unambiguously the depth at which thrusts sole out, the data suggest that some thrust faults penetrate close to the top of the subducting ocean crust. Thrust faults and related anticlines are spaced at roughly 5 km perpendicular to the margin. Parallel to the margin, there are significant variations both in the amount of displacement along a fault and in the style of deformation. Subsidiary backthrusts propagating upward from the frontal thrust are sometimes observed, but on nearby lines the equivalent faulting is absent and deformation is accomplished by folding. Such variations imply that there may be localized variations of pore-fluid pressure. In one region where the sediment wedge taper is very small, high pore fluid pressures along the detachment surface are inferred. Strong near-basement reflections beneath the deformation front are also indicative of high fluid pressure.

The landward extent of accreted sediments is limited by the marine volcanic Crescent Terrane, which dips toward the continent and can be traced close to the top of the subducting oceanic crust. High pore pressures may exist at the base of the sediment wedge near the backstop, where bright near-horizontal reflections are observed similar to those seen beneath the deformation front of the shallow-taper wedge region. The Crescent Terrane appears to have been tilted landward, perhaps associated with the accretion of prism sediments. The pattern of tilting suggests that uplift may have occured by imbrication within the Crescent Terrane.

Acknowledgements. The seismic program was supported by the Geological Survey of Canada. Data collection was contracted to Digicon (Canada) Inc., and we gratefully appreciate the efforts of the personnel onboard the M/V GEOTIDE. Data processing was performed by Geophoto Ltd of Calgary. Kristin Rohr at PGC provided useful advice during the processing of the data. The authors are particularly grateful to R. von Huene for a substantive critical review. Support for GDS derived from Grant URF0043000 of the Natural Sciences and Engineering Research Council. Geological Survey of Canada contribution 57290.

References

Calvert, A.J. and Clowes, R.M., Seismic constraints on fluid flow within the accretionary complex of western Canada (submitted).

Clowes, R.M., Brandon, M.T., Green, A.G., Yorath, C.J., Sutherland Brown, Kanasewich, E.R. and Spencer, C., LITHOPROBE - southern Vancouver Island: Cenozoic subduction complex imaged by deep seismic reflections, *Can. J. Earth Sci., 24*, 31-51, 1987.

Davis, E.E. and Hyndman, R.D., Accretion and recent deformation of sediments along the northern Cascadia subduction zone, *Geol. Soc. Am. Bull., 101*, 1465-1480, 1989.

Davis, D., Suppe, J. and Dahlen, F.A., Mechanics of fold and thrust belts and accretionary wedges, *J. Geophys. Res., 88*, 1153-1172, 1983.

Davis, E.E., Hyndman, R.D. and Villinger, H., Rates of fluid expulsion across the northern Cascadia Accretionary prism: constraints from new heat flow and multichannel seismic reflection data, *J. Geophys. Res., 95*, 8869-8889, 1990.

Green, A.G., Clowes, R.M., Yorath, C.J., Spencer, C., Kanasewich, E.R., Brandon and A. Sutherland Brown, Seismic reflection imaging of the subducting Juan de Fuca plate, *Nature, 319*, 210-213, 1986.

Green, A.G., Milkereit, B., Mayrand, L., Spencer, C., Kurtz, R. and Clowes, R.M., LITHOPROBE seismic reflection profiling across Vancouver Island: results from reprocessing, *Geophys. J., 89*, 85-90, 1987.

Hyndman, R.D., Yorath, C.J., Clowes, R.M. and Davis, E.E., The northern Cascadia subduction zone at Vancouver Island: Structure and tectonic history, *Can. J. Earth Sci., 27*, 313-329, 1990.

Hyndman, R.D. and Davis, E.E., A mechanism for the formation of methane hydrate and sea floor bottom simulating reflectors by vertical fluid expulsion, *J. Geophys. Res.* (in press).

MacKay, M., Cochrane, G., Moore, G.F. and Kulm, L.D., High resolution seismic survey of the Oregon accretionary prism, *Trans. AGU, 70*, 1345, 1989.

Massey, N.W.D., The Metchosin Igneous Complex, southern Vancouver Island; ophiolite stratigraphy developed in an emergent island setting, *Geology, 14*, 602-605, 1986.

McCarthy, J. and Scholl, D.W., Mechanisms of subduction accretion along the central Aleutian trench, *Bull. Geol. Soc. Am., 96*, 691-701, 1985.

Moore, G.F. and Shipley, T.H., Mechanics of sediment accretion in the Middle America Trench off Mexico, *J. Geophys. Res., 93*, 8911-8927, 1988.

Moore, G.F., Shipley, T.H., Stoffa, P.L., Karig, D.E., Taira, A., Kuramoto, S., Tokuyama, H., and Suyehiro, K., Structure of the Nankai Trough accretionary zone from multichannel seismic reflection data, *J. Geophys. Res., 95*, 8753-8765, 1990.

Shouldice, D.H., Geology of the western Canadian continental shelf, *Bull. Can. Petr. Geol., 19*, 405-436, 1971.

Waldron, D.A., Clowes, R.M. and White, D.J., Seismic structure of a subducting oceanic plate off western Canada, in *Studies of laterally heterogeneous structures using seismic refraction and reflection data*, edited by A.G. Green, *Geol. Surv. Can., Paper 89-13*, 1989.

Westbrook, G.K. and Smith, M.J., Long décollements and mud volcanoes: evidence from the Barbados Ridge Complex for the role

of high pore-fluid pressure in the development of an accretionary complex, *Geology, 11*, 279-283, 1983.

TABLE 1. Fault displacements (m) along landward dipping thrust faults at the deformation front. Displacements are measured near the base of the turbidite layer.

	Line			
Fault	89-03	85-01	89-04	89-05
LDF1	280	400	620	1000
LDF2	1150	1000	1000	950
LDF3	-	50	250	330

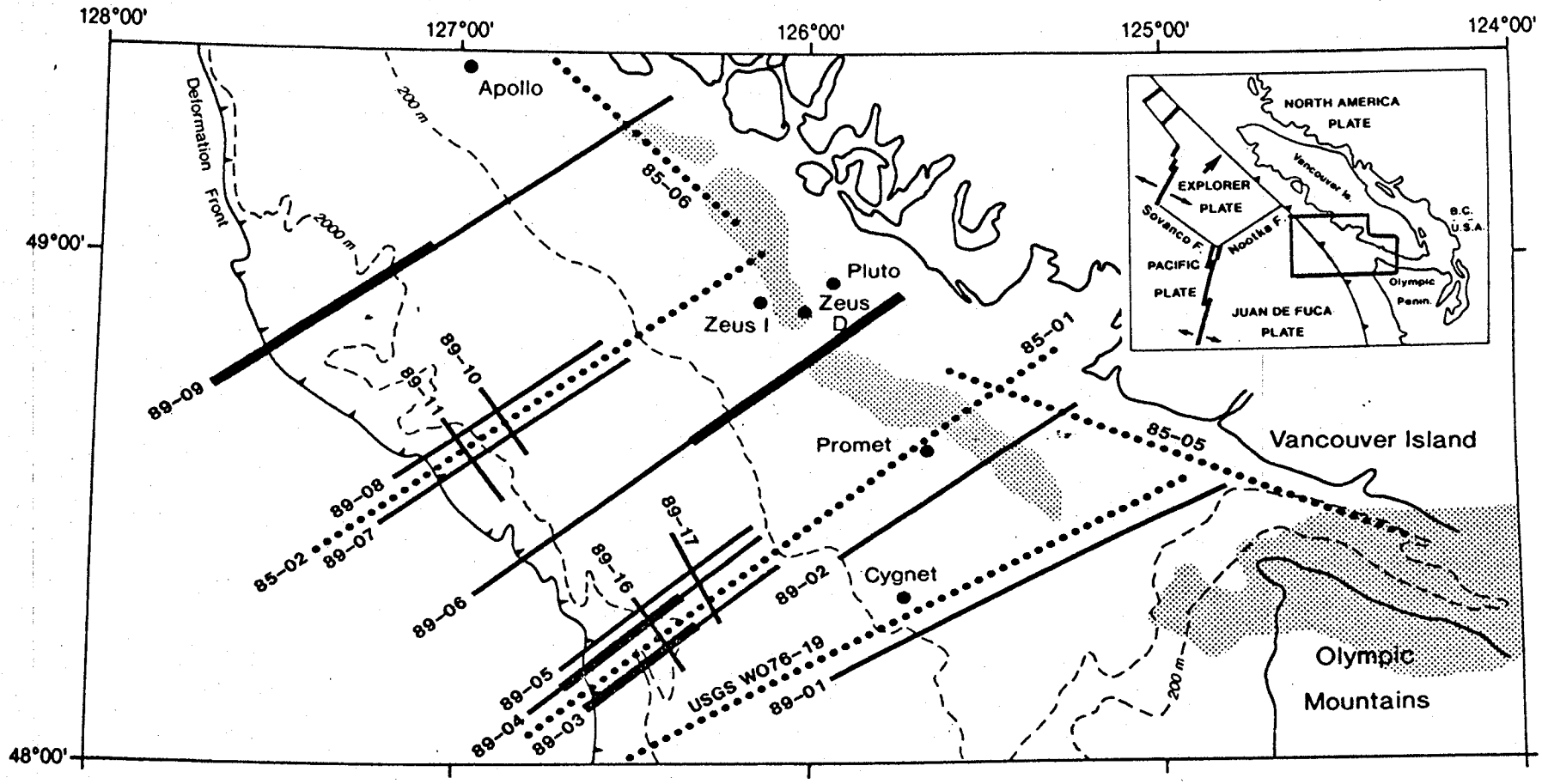
128°00'
127°00'
126°00'
125°00'
124°00'
49°00'
48°00'
Deformation Front
200 m
2000 m
Apollo
85-06
Pluto
Zeus D
Zeus I
89-09
89-10
89-11
89-08
89-07
85-02
89-06
89-17
89-16
89-05
89-04
89-03
USGS WO76-19
89-02
89-01
85-01
85-05
Promet
Cygnet
Vancouver Island
Olympic Mountains
200 m
NORTH AMERICA PLATE
EXPLORER PLATE
Sovanco F.
Nootka F.
PACIFIC PLATE
JUAN DE FUCA PLATE
Vancouver Is.
B.C.
U.S.A.
Olympic Penn.

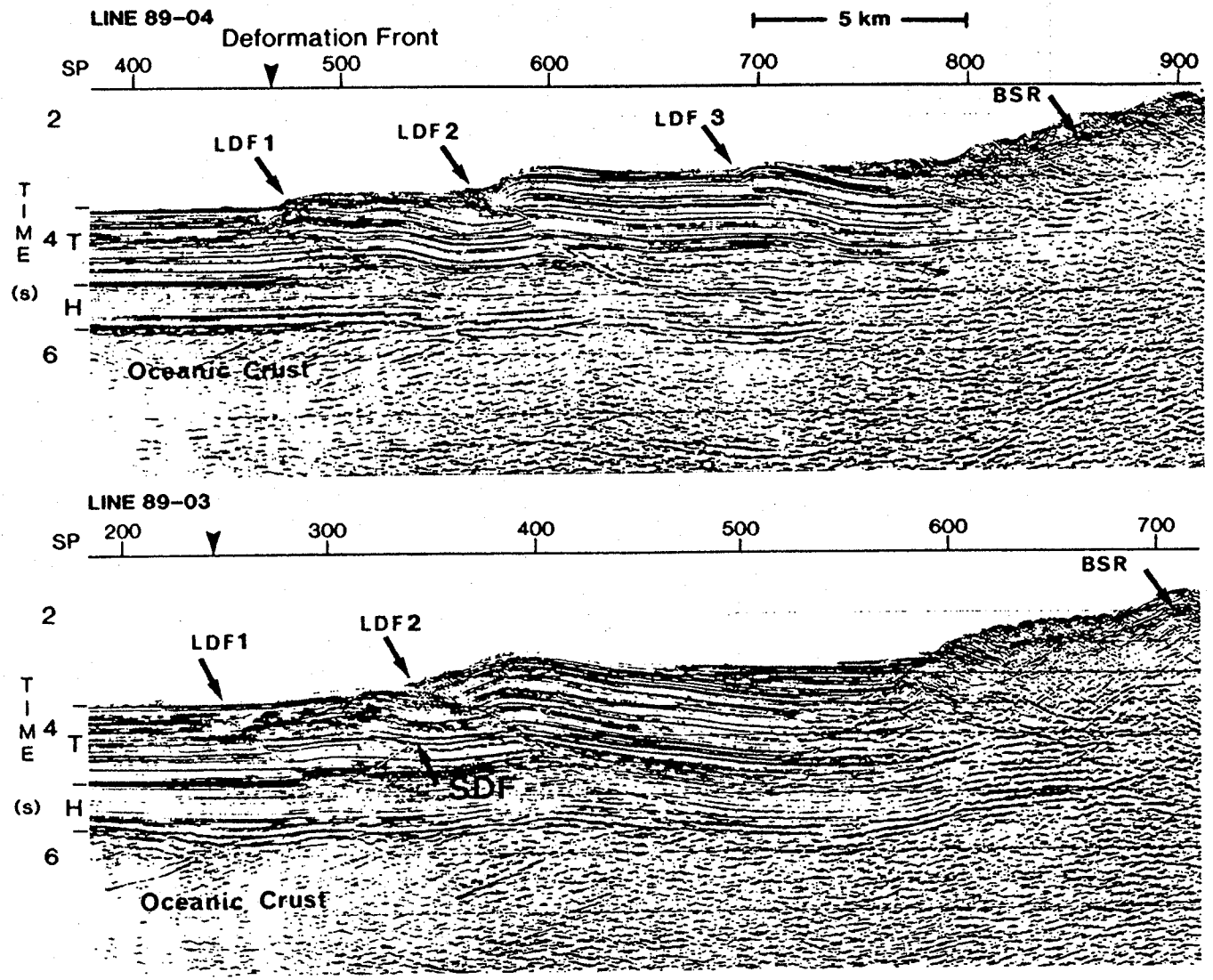
LINE 89-04
Deformation Front
5 km
SP 400 500 600 700 800 900
BSR
LDF 1
LDF 2
LDF 3
TIME (s)
2
4 T
H
6
Oceanic Crust
LINE 89-03
SP 200 300 400 500 600 700
BSR
LDF1
LDF2
SDF
2
4 T
H
6
Oceanic Crust

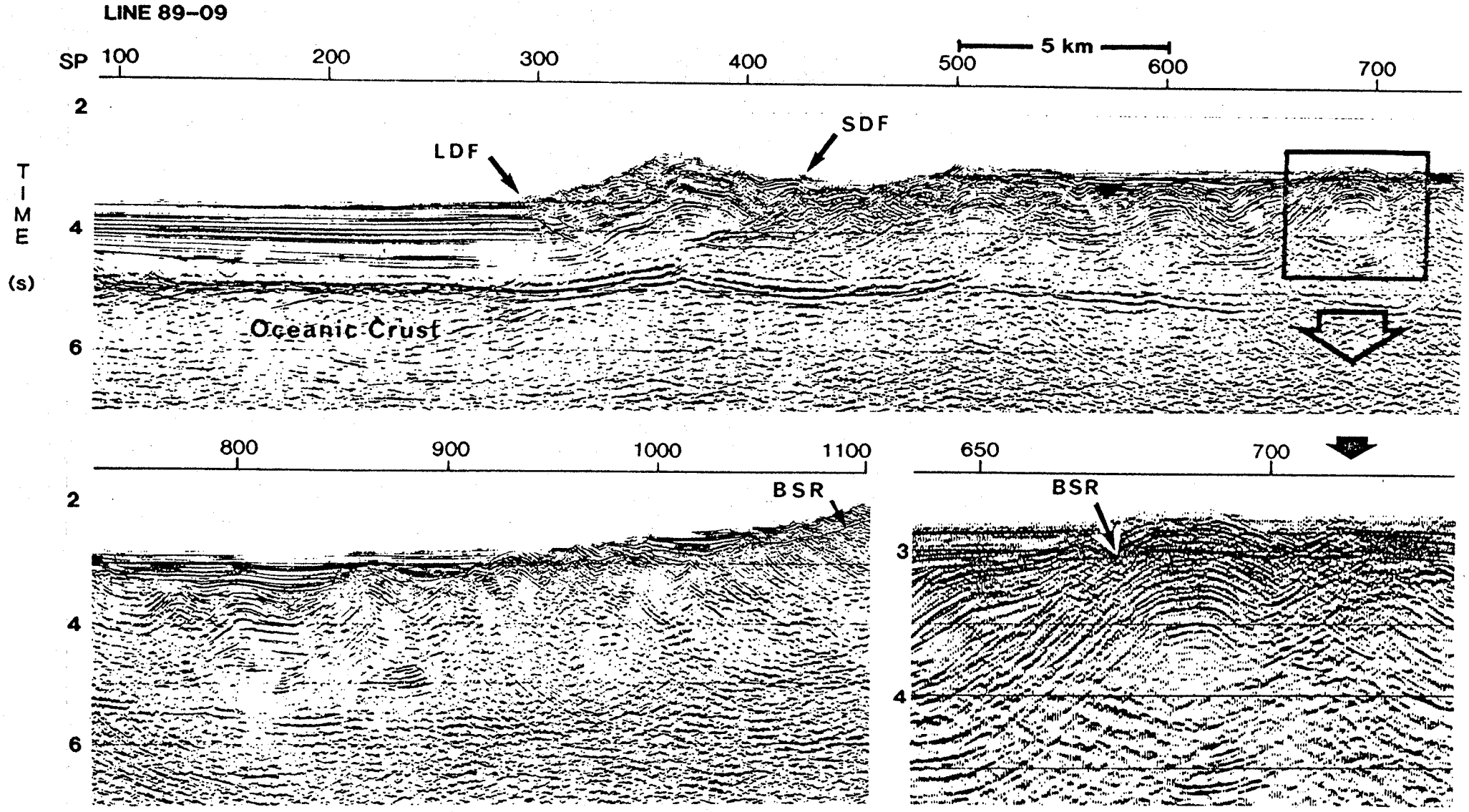
LINE 89-09
SP
100
200
300
400
500
5 km
600
700
2
4
6
TIME
(s)
LDF
SDF
Oceanic Crust
800
900
1000
1100
650
700
BSR
BSR
2
4
6
3
4

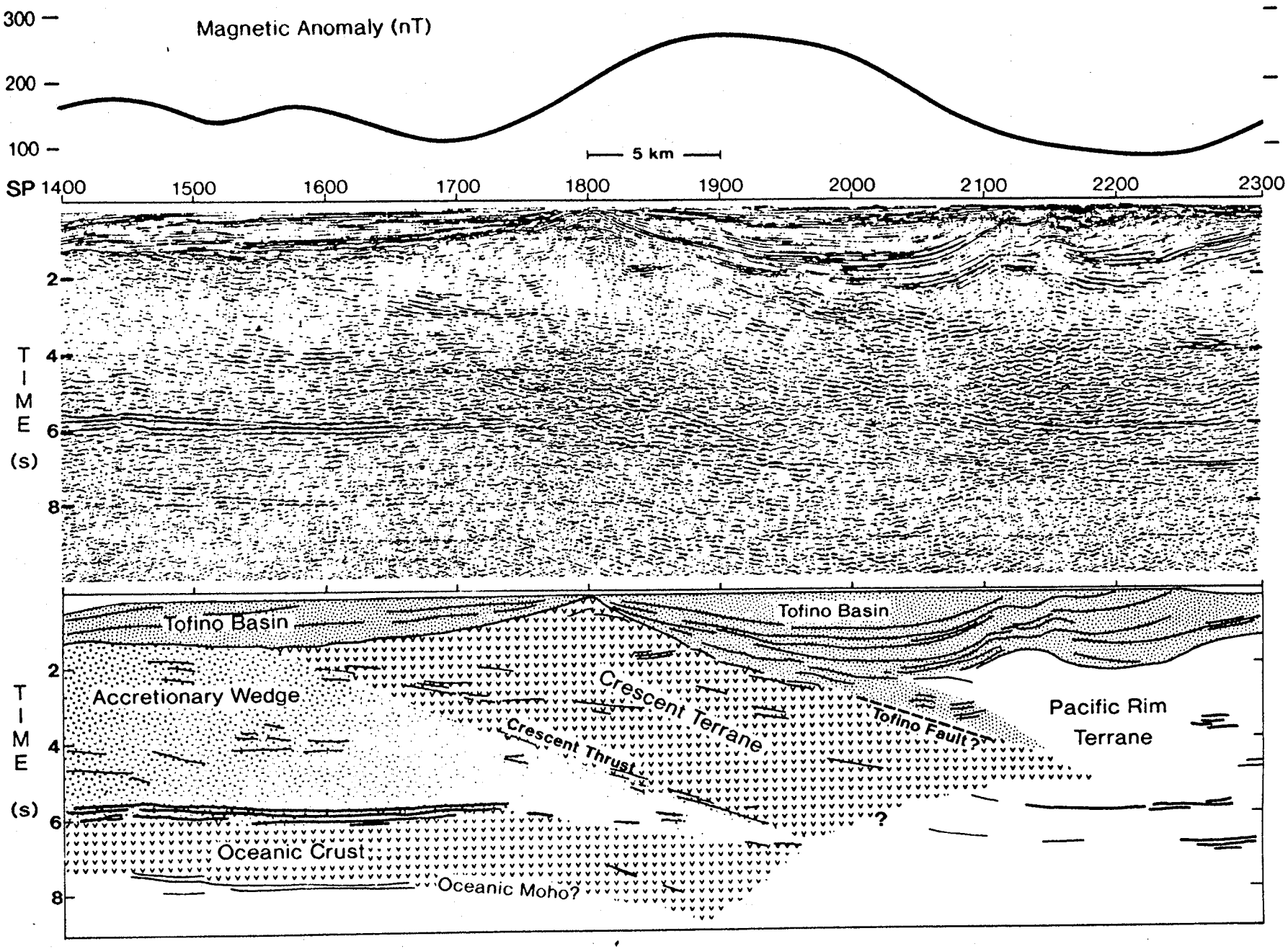
LINE 89-06
300
Magnetic Anomaly (nT)
200
100
5 km
SP 1400
1500
1600
1700
1800
1900
2000
2100
2200
2300
TIME (s)
2
4
6
8
Tofino Basin
Tofino Basin
Accretionary Wedge
Crescent Terrane
Crescent Thrust
Tofino Fault?
Pacific Rim Terrane
?
Oceanic Crust
Oceanic Moho?